Non-invasive electrocardiographic imaging in patients with idiopathic ventricular fibrillation

An algorithm for calculating repolarization parameters

B.M. Wulterkens

Master's Thesis
Technical Medicine

General information

Title	Non-invasive electrocardiographic imaging in patients with ventricular fibrillation: An algorithm for calculating repolarization parameters
Author	B.M. Wulterkens
Student number	s1390031
E-mail	wulterkensbernice@gmail.com
Date	1st of February 2019

Organization

Address	University Medical Center Utrecht Heidelberglaan 100 3584 CX Utrecht
Department	Department of Cardiology

Institution

Address	University of Twente Drienerlolaan 5 7522 NB Enschede
Faculty	TNW: Science and Technology
Master	Technical Medicine

Graduation committee:

Chair and technical supervisor	Prof.dr.ir. C.H. Slump
Clinical supervisor	Dr. R.J. Hassink
Clinical/technical supervisor	Drs. L.J. Blom
Process supervisor	Drs.R.J. Haarman
External member	Dr. E.J.F.M. ten Berge

UMC Utrecht

UNIVERSITY OF TWENTE.

Summary

Idiopathic ventricular fibrillation (IVF) is diagnosed in patients who have survived a ventricular fibrillation (VF) episode without any identifiable structural, electrical or metabolic cause. Recently, a research project has started to identify possible substrates that can elucidate the development of VF in IVF using electrocardiographic imaging (ECGI). ECGI is a method used for non-invasive epicardial electrophysiologic mapping.

The purpose of this study was to develop a method for (semi-)automatic calculation of repolarization parameters in unipolar electrograms reconstructed with ECGI. Repolarization parameters include Tpeak-Tend (Tp-e) interval, T-wave area, T-wave amplitude and T-wave alternans. The algorithm was validated against two observers and achieved a maximum sensitivity of 93.5% and 27.5% for the (primary) T-peak and T-end respectively. A tool for detailed representation of the calculated repolarization parameters on each reconstructed electrogram is included for reliable interpretation of the results.

The algorithm was applied on ECGI-data of five patients with IVF and one control subject. We showed that it is possible to visualize epicardial repolarization parameters using ECGI. The results suggest that Tp-e intervals and T-wave alternans measured with ECGI can provide information about the substrate for the development of VF in IVF and provides a foundation for further exploration of the repolarization characteristic in a larger study population and in control subjects. To our knowledge, this is the first study that uses alternative repolarization parameters measured with ECGI.

Furthermore, the presence of late gadolinium enhancement (LGE) on cardiac magnetic resonance (CMR) imaging has been visualized using the software program CARTBox. The results indicate the diversity in the location and the extent of transmurality of LGE between the subjects. The obtained 3D reconstructions enable comparison of LGE regions with 3D images obtained by ECGI. The possibility to correlate LGE regions with deviating areas measured with ECGI may lead to treatment of these regions with local therapy, such as ablation therapy or the choice for a drug with a specific pathway.

Preface

Voor u ligt mijn afstudeerthesis van de master Technical Medicine, richting Medical Sensing & Stimulation, aan de Universiteit Twente. De afgelopen tien maanden heb ik stagegelopen op de afdeling Cardiologie in het Universitair Medisch Centrum Utrecht waar ik met veel plezier aan dit afstudeeronderzoek heb gewerkt. Vele mensen hebben bijgedragen aan de totstandkoming van deze thesis, die ik bij deze graag zou willen bedanken.

Allereerst wil ik mijn medisch begeleider, Rutger, bedanken voor het mogelijk maken om af te studeren binnen het onderwerp waar voor mij een grote interesse ligt. Je deur stond altijd voor me open en met vragen kon ik altijd bij je terecht.

In het bijzonder wil ik Lennart bedanken voor de dagelijkse begeleiding en de kritische blik met betrekking tot mijn onderzoek. We hebben regelmatig kunnen sparren over het onderzoek en methodes die we konden toepassen voor de verbetering in het script. Ik wil je graag bedanken voor je toegankelijkheid en het gevoel van vertrouwen dat je mij gaf. Verder wil ik graag alle mensen op de afdeling en in Q5 bedanken voor de gezellige tijd. Ik heb me erg met jullie vermaakt.

Kees wil ik graag bedanken voor de technische begeleiding vanuit de Universiteit Twente. Jouw kritische kijk op de methode heeft mij steeds weer op scherp gezet. Ook wil ik je bedanken voor het delen van de mooie uitspraak "*de humor van het leven*". Deze zorgt er regelmatig voor dat het maken van een keuze toch net iets makkelijker wordt.

Rian, ik wil jou graag bedanken voor de vele inzichten die je mij hebt gegeven de afgelopen twee jaar. Je wist altijd met de juiste vragen de gevoelige snaar te raken. Dit heeft geleid tot een mooie persoonlijke ontwikkeling en mijn ontwikkeling als technisch geneeskundige, waar ik trots op mag zijn.

Erik, bedankt voor het leuke onderwijs dat ik de afgelopen jaren bij jou heb mogen volgen, ik heb ontzettend veel van je geleerd. Daarnaast wil ik je natuurlijk ook bedanken voor het vervullen van de plek als buitenlid in mijn afstudeercommissie.

Naast mijn directe begeleiding wil ik Matthijs, Bianca en Job bedanken voor het aanleveren van de data en het enthousiast meedenken over het project.

Niet te vergeten dat ook mijn lieve vriendinnen een bijdrage hebben geleverd aan dit alles. Samen met jullie heb ik de afgelopen zes jaar ontzettend veel geleerd en veel plezier gehad, waar een bijzondere vriendschap uit is ontstaan. Maar natuurlijk hebben jullie ook support gegeven tijdens de afgelopen stages en ook dit afstudeerjaar. Heel erg bedankt lieve Lieke, Liset en Marijn.

Tevens wil ik mijn lieve mama, Jack, en zusjes bedanken voor alle oprechte interesse, energie en de gegeven adviezen de afgelopen jaren. Ik waardeer het enorm dat jullie altijd achter mijn keuzes hebben gestaan en het vertrouwen in mij hebben gehad. Opa en oma, jullie wil ik ook graag bedanken

voor de heerlijke vakantie die we samen hebben gehad in Oostenrijk. Deze week heeft ervoor gezorgd dat ik het laatste deel van mijn afstudeerjaar succesvol en met veel energie kon volbrengen.

Leendert, zonder jouw onvoorwaardelijke steun en positieve energie was dit alles ook zeker niet mogelijk geweest. Aan jouw blik op zaken heb ik erg veel gehad. Fijn dat ik altijd bij je terecht kon, dat je altijd voor mij klaar staat en overal een positieve draai aan weet te geven.

Bernice Wulterkens
Utrecht, Januari 2019

List of abbreviations

3D	Three Dimensional
AUMC	Amsterdam University Medical Center
BrS	Brugada syndrome
CMR	Cardiac Magnetic Resonance
CPVT	Cathecholaminergic polymorphic ventricular tachycardia
CT	Computed Tomography
DWT	Discrete Wavelet Transform
ECGI	Electrocardiographic imaging
ECG	Electrocardiogram
ERP	Early Repolarization Pattern
ERS	Early Repolarization syndrome
ICD	Implantable Cardioverter Defibrillator
IVF	Idiopathic ventricular fibrillation
LGE	Late Gadolinium Enhancement
LQTS	Long QT syndrome
LV	Left Ventricle
M cells	Myocardial cells
MRI	Magnetic Resonance Imaging
MUMC	Maastricht University Medical Center
RV	Right Ventricle
SCA	Sudden cardiac arrest
SWT	Stationary Wavelet Transform
TdP	Torsade de Pointes
Tp-e	Tpeak-Tend
UMCU	University Medical Center Utrecht
VF	Ventricular fibrillation
WT	Wavelet Transform

Contents

Introduction

1 Clinical context

Sudden cardiac arrest (SCA) is the most common lethal manifestation of heart disease, with an estimated incidence of 1 per 1,000 person-years in the general Dutch population [1]. SCA refers to a natural and unexpected collapse of presumed cardiac etiology. A rare cause of SCA is idiopathic ventricular fibrillation (IVF). IVF is diagnosed in patients who have survived a ventricular fibrillation (VF) episode without any identifiable structural, electrical or metabolic causes despite extensive diagnostic testing. In 2013, IVF was defined as *'a resuscitated cardiac arrest victim, preferably with documentation of VF, in whom known cardiac, respiratory, metabolic and toxicological causes have been excluded through clinical evaluation'*.[2] This reflects the current inability to establish a link between a life-threatening arrhythmic event and clinical information obtained by detailed invasive and non-invasive examination.

The prevalence of idiopathic ventricular fibrillation in the Netherlands is unknown, but it is estimated at 1,000 patients [3]. IVF is a diagnosis *per exclusionem* and the certainty of the diagnosis depends on the extent of diagnostic workup performed to exclude underlying causes. In 7 to 35% of the cases, patients reveal a different diagnosis during follow up due to disease progression or more extensive or advanced clinical evaluation. [4]

Usually, patients with SCA without underlying heart disease are younger than 40 years [3]. Because of the absence of a known arrhythmogenic substrate in patients with IVF, we are unable to both identify those patients at risk and give advice to family members concerning their future risk of events.

Recently, the VIGILANCE project has started and comprises a collaboration between the University Medical Center Utrecht (UMCU), Maastricht University Medical Center (MUMC) and Amsterdam University Medical Center (AUMC). The project focusses on the use of non-invasive electrocardiographic imaging (ECGI) in patients with IVF and their relatives. It has been demonstrated that ECGI can elucidate arrhythmogenic substrates in the human heart [5]–[7]. The aim of the VIGILANCE project is to gain insight in the electrical activity of the heart and to expose a potential underlying arrhythmogenic substrate responsible for the occurrence of VF in these patients. In addition, opportunities for risk stratification of family members will be investigated.

2 Research purposes

At the moment, the traditional 12-lead electrocardiogram (ECG) is used to define abnormalities in cardiac electrical activity by calculation of repolarization parameters such as the QT interval, QT dispersion and Tpeak-Tend interval. It is hypothesized that a mechanism for development of VF in IVF can be a result of repolarization abnormalities, but at this moment, these cannot be exposed by diagnostic testing [8]. According to several studies, the introduction of ECGI creates opportunities to gain insight in the electrical activity of the heart at the epicardial level [7], [9], [10]. At the moment, ECGI is mainly used for local determination of activation and recovery times, but not for the analysis of repolarization parameters that are used in the 12-lead ECG. It is hypothesized that these repolarization parameters can reveal potential arrhythmogenic substrates in IVF, using non-invasive ECGI. The primary aim of this study was to develop a method for accurate measurement of T-wave parameters in epicardial unipolar electrograms calculated with non-invasive ECGI.

In patients with IVF, extensive diagnostic testing did not provide an apparent pathogenesis. However, some tests show small abnormalities, but these are insignificant to define an underlying diagnosis. An example of an abnormality is Late Gadolinium Enhancement (LGE) on cardiac magnetic resonance (CMR) imaging. In the UMCU and the MUMC, the data of nine patients that are diagnosed with IVF show LGE on CMR. It is hypothesized that LGE includes information about the arrhythmogenic substrate in IVF. Therefore, the second aim of the study was to provide an overview of regions of LGE on CMR in patients with IVF.

The mentioned aims can be translated into two main research questions and corresponding sub questions:

Research question 1:
Is it possible to identify arrhythmogenic substrates by measuring repolarization parameters on the epicardium in patients with idiopathic ventricular fibrillation using non-invasive electrocardiographic imaging?

Sub question 1: Is it possible to develop an accurate method to measure various T-wave parameters on electrograms acquired by non-invasive electrocardiographic imaging?

Sub question 2: How are these parameters expressed on the epicardium in a control subject?

Sub question 3: Do these parameters show abnormalities on the ventricular epicardium in patients with idiopathic ventricular fibrillation?

Sub question 4: Is it possible to correlate abnormalities with the risk of occurrence of ventricular fibrillation?

Research question 2:
Is it possible to visualize regions with late gadolinium enhancement on cardiac magnetic resonance imaging in such a way that it enables comparison with results from non-invasive electrocardiographic imaging?

3 Thesis outline

The first chapter described the clinical need for this project. A brief introduction on idiopathic ventricular fibrillation (IVF) was given as well as the aim of this thesis with corresponding research questions. In chapter 2, a more detailed background about IVF, electrocardiographic imaging (ECGI) and the use of cardiac magnetic resonance (CMR) in patients with IVF is given. Chapter 3 will describe the developed algorithm for calculation of repolarization parameters in unipolar epicardial electrograms reconstructed with ECGI. Furthermore, validation of the algorithm is reported. Chapter 4 includes the results of the implementation of the algorithm on ECGI-data of five patients with IVF and one control subject. Chapter 5 will describe a method for late gadolinium enhancement (LGE) on CMR in patients with IVF. In chapter 6 the main findings of this research project will be summarized and future perspectives will be discussed.

Background

1 Idiopathic ventricular fibrillation

1.1 Pathophysiology

Over the last decades, at least five primary arrhythmia syndromes were discovered, which were considered as IVF before. For example, the Brugada Syndrome (BrS), early repolarization syndrome (ERS) and short-QT syndrome were described as IVF earlier, but the presence of a distinct pathophysiology and disease entity resulted in a different diagnosis [11]–[14]. Moreover, the advance in genetic testing has resulted in discovery of other primary arrhythmic syndromes in other IVF cases, such as catecholaminergic polymorphic ventricular tachycardia (CPVT) and long QT syndrome (LQTS). [15] Genetic testing has also exposed causative mutations for IVF such as the Dutch *DPP6*-haplotype and *CALM1* gene.[16], [17]

This demonstrates that the IVF population is a heterogeneous group and various underlying substrates may cause the arrhythmic event, what makes it difficult to understand the mechanisms involved in IVF. A number of primary arrhythmia syndromes, that were initially defined as IVF, result in repolarization abnormalities. This hypothesizes that this can play a role in other IVF cases.

Repolarization

Heterogeneity of ventricular repolarization is associated with malignant ventricular arrhythmias, such as VF and Torsades de Pointes (TdP). [18], [19] The ventricular myocardium includes three types of cells: endocardial, epicardial and myocardial (M) cells. These cells are structurally similar but have different electrophysiological characteristics. For example, M cells have longer action potentials compared with epicardial and endocardial cells [20], [21]. This is due to a delay or blockage of K^+ and an increase in Na^+ currents [22]. In normal conditions, the physiological differences among these cells are minimized by electronic influences from well coupled myocytes [23]. The T-wave in the ECG reflects the repolarization period of the heart cycle (see Figure 1). The height and width of this part of the ECG is determined by the interaction between opposing transmural forces among the cells in the ventricular myocardium [22]. Multiple conditions, for example electrolyte disturbances, cause pathophysiological changes with alteration

in the normal pattern of repolarization, increasing heterogeneity and the risk of developing malignant ventricular arrhythmias.[24] An example of an alteration in the repolarization pattern is ERS. This can be seen on the 12-lead ECG as an elevated J-point in ≥2 leads from the same regional territory [25]. Haïssaguerre et al. demonstrated an increased prevalence of early repolarization among patients with a history of IVF [26]. Next to that, it seems that the early repolarization pattern (ERP) is highly predictive for arrhythmia recurrence in patients with IVF [27], [28]. A recent study revealed the presence of an abnormal electrophysiological substrate in ERS patients, characterized by steep repolarization gradients. These regions may be caused by spatially heterogeneous shortening of the action potential over small distances and provide a substrate that is susceptible to the development of asymmetrical conduction and re-entrant arrhythmias including VF. It remains unclear whether these mechanisms explain the increased mortality associated with ERP [29]. Understanding the mechanism of early repolarization and how it may predispose patients to an increased risk of arrhythmias requires detailed information of the electrophysiological substrate in the intact heart of ERS patients.

Intracardiac mapping studies revealed conduction and repolarization abnormalities in patients with channelopathies such as BrS and also in IVF, although it is unclear if these abnormalities are associated with risk of SCA [30], [31]. Recently, the role of repolarization abnormalities during exercise was investigated in SCA survivors with structurally normal hearts, using ECGI. Regions of delayed activation following exercise were seen more frequently in patients with IVF compared to controls. This can create a substrate for reentry in individuals with increased dispersion of repolarization.[9] In IVF, this uniformity might be due to abnormal repolarization of the preceding local action potential, an unidentified channelopathy or inherent structural abnormalities not detectable on magnetic resonance imaging (MRI) [32]. These results suggest that IVF might be due to abnormalities in the repolarization dispersion.

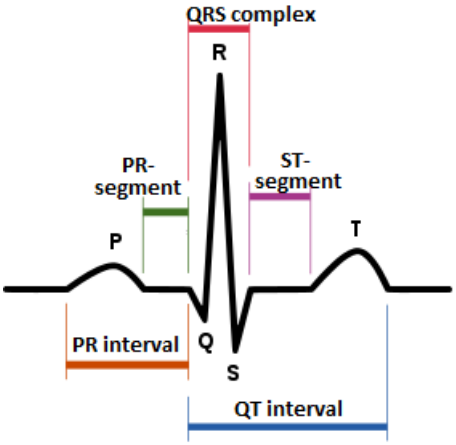

Figure 1 An example of the ECG of a single heartbeat, modified from [33]

1.2 Diagnosis

The correct diagnosis of IVF requires extensive diagnostic testing. Common causes of VF can be excluded by routine testing, including blood chemistry, toxicological screening, ECG, chest X-ray, echocardiography, exercise testing, Holter or telemetry monitoring, coronary angiography with or without ventriculography, and MRI. Recommended additional tests include ergonovine or acetylcholine provocation to exclude coronary artery spasm and administration of a sodium channel blocker to exclude BrS. However, when IVF occurs in families, it is difficult to identify family members at risk for IVF, because no clinical parameters to guide risk stratification have yet been defined.[16], [34] It is valuable to identify patients with potential substrates and to stratify their risk of developing malignant arrhythmias. This can lead to early recognition of these patients and treatment or prevention of life-threatening events.

1.3 Treatment

Therapy in IVF is still a challenge to cardiologists and electrophysiologists. Nowadays, limited data are available concerning SCA risk stratification and the strategy for primary prevention of SCA in IVF had not been established in persons at risk, such as family members of patients with IVF. For secondary prevention, implantable cardioverter defibrillator (ICD) therapy represents the therapy of choice. It has been demonstrated that 20-30% of IVF patients suffer from recurrence of VF and receive an appropriate ICD shock [4], [35]. This indicates that a part of

the IVF population suffers from VF only one time in his life and that risk classification will have to improve to treat patients in an optimal way.

1.4 Non-invasive electrocardiographic imaging (ECGI)

The development of new diagnostic tools is necessary to further unravel the arrhythmogenic substrate in patients with IVF.

For decades, the ECG is used to determine normal cardiac activation and repolarization, but also abnormalities of the heart. It represents the cardiac electrical activity on the body surface, not on the heart itself. This limits the spatial resolution for determination of regional cardiac electrical activity and the ability to locate regions of arrhythmic activity. Regional cardiac electrical activity can be established using ECGI. A novel tool with the advantage of providing more detailed, regional information on depolarization and repolarization patterns on the epicardial surface of the heart.[9] ECGI's ability to assess depolarization and repolarization more accurately has been validated and results indicate that this method can be used to detect and locate arrhythmogenic substrate by capturing potentials, electrograms and activation sequences on the epicardium [36], [37]. The added value to establish repolarization abnormalities that are potential substrates inducing malignant arrhythmias has been provided by different researchers [5], [38], [39]. This can contribute to 1) the identification of patients at risk for sudden death, 2) providing a specific diagnosis to indicate specific treatment strategy, 3) guiding a therapeutic intervention (e.g. ablation) to the optimal location in the heart, and 4) the evaluation of the outcome of treatment (e.g. drug therapy) during follow-up.

ECGI in healthy individuals and in patients with primary arrhythmia syndromes

ECGI has been studied in various populations, including healthy individuals and patients with primary arrhythmia syndromes. In healthy subjects, it was demonstrated that the repolarization sequence was determined by local repolarization properties rather than by activation sequence. Besides, significant dispersion of repolarization was observed between the right and left ventricle, and from apex to base. It was suggested that local action potential duration (local repolarization) is the major determinant of the repolarization sequence in the normal human heart.[40]

Studies with ECGI demonstrated increased dispersion of repolarization in several arrhythmogenic diseases. For example in patients with BrS, regions of prolonged repolarization and steep repolarization gradients were identified in the right ventricular outflow tract.[30] Patients with LQTS revealed a marked increase in heterogeneity of ventricular recovery on the epicardium which caused significant delay in repolarization in certain regions resulting in abnormally steep repolarization gradients. In addition, repolarization gradients were steeper in symptomatic patients, suggesting that increased dispersion may be predictive for arrhythmia risk.[41] Patients with an early repolarization pattern and sudden unexplained cardiac arrest showed normal ventricular activation, although abnormal repolarization was identified and characterized by areas with short intervals between activation and recovery.[42] These outcomes suggest that ECGI can play a crucial role in the detection of malignant arrhythmogenic substrates in patients with IVF.

The concept of ECGI

Excitation of the heart generates an electric potential field, ϕ, between the epicardium and the body surface, and can be described by the following (Laplace) equation:

$$\nabla^2 \phi = 0 \tag{1}$$

Where ∇^2 is the Laplacian operator; ϕ is defined as the electric potential field and can either be defined on the torso surface, ϕ_T, or on the epicardium, ϕ_E. ϕ_T can be measured non-invasively by electrodes placed on the body surface.[6] The intention of ECGI is to compute ϕ_E from the measured ϕ_T, also called the inverse problem of electrocardiography, which describes the propagation of electromagnetic activity from the body surface to the heart. This inverse model is based on a forward model with known 'output' and unknown 'source', see Figure 2. The forward model can be described by the following matrix equation:

$$\phi_T = A\phi_E \tag{2}$$

where ϕ_T is a vector of measured torso potentials (model output), ϕ_E is a vector of unknown epicardial potentials (cardiac source) and matrix A contains the geometric information that relates the heart and torso surfaces (the electromagnetic

source-output relation) [6], [38]. A fourth element is required to solve the inverse problem and compute ϕ_E from a known ϕ_T, namely regularization methods. This is necessary because the reconstruction is highly sensitive to noise [38].

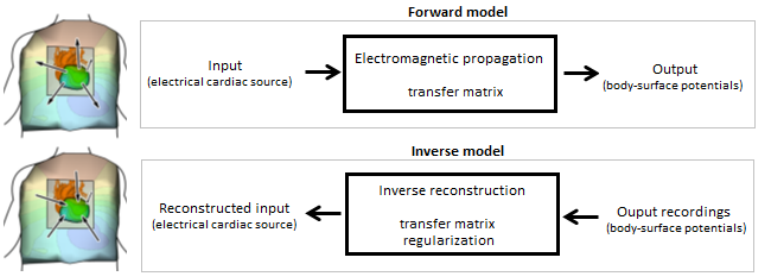

Figure 2 Schematic representation of forward/inverse models. A forward model describes the propagation of electromagnetic activity from the heart to the body surface; an inverse model reverses that relation, allowing for non-invasive reconstruction of electrical heart activity from measured body-surface potentials. [38]

The first step in ECGI is to measure the electrical potentials on the patient's torso using a minimum of 59 electrodes [43]. The electrodes are connected to a multichannel mapping system (Active Two system BioSemi B.V., Amsterdam). All measured body-surface potentials are filtered by an anti-aliasing filter using a fixed first order analog filter and stored in a Binary Data File (BDF file).

The electrical activity of the heart (ϕ_E, the cardiac source) is described by a mathematical model and is based on the integral relationship between epicardial and body surface potentials [44]. Local electrograms at the epicardium are reconstructed in this model, from which additional information can be obtained, such as activation and repolarization times.

The next step is to determine the electromagnetic relation between source and output, captured by a patient-specific matrix (A). The matrix is based on the conductivity and geometry of the patient's torso, and is necessary for creating accurate, patient-specific reconstructions that can be linked to anatomical location and abnormalities. The anatomical reference can be obtained by a computed tomography (CT), from which a geometry is created that consists of the heart surface defined by the epicardium, the location of body-surface electrodes and the torso-volume conductor properties, such as the conductivity of blood and torso (which is assumed to be homogeneous). First, the epicardium of the ventricles and the location of the body-surface electrodes are segmented manually from the CT-scan using the open source software program Seg3D [45]. Subsequently, a mesh of the heart and torso surface is created using triangular elements. The patient-specific

matrix is derived using boundary element algorithms which relate body surface potentials to epicardial potentials.

Finally, to reconstruct the cardiac electrical activity, regularization methods need to be applied because the inverse problem is inherently ill-posed. This means that the solution of the problem is sensitive to small perturbations in the measured body-surface potentials, such as noise. Low levels of signal noise or small geometric error can result in an unbounded solution. Ill-posedness is known as the mathematical result of the attenuating and distributing effect of the electromagnetic propagation from heart to body surface, what can lead to numerical instability [46]. To deal with this uncertainty and sensitivity of inverse models, so-called 'regularization-methods' can be applied. In regularization, constraints are applied to the solutions based on physical or mathematical properties that are not yet incorporated in the transfer matrix. This additional information will increase reliability [47]. Various regularization methods are available, such as truncated Singular Value Decomposition (tSVD), Greensite SVD, and the Generalized Minimal Residual (GMRes) method. An often-used regularization method is called Tikhonov regularization and the zero-order Tikhonov method is used in this method for ECGI. This method assumes that epicardial potentials should be reasonably small. Tikhonov regularization calculates the minimum-norm least squares, following:

$$f\ \varphi_E\ =\ \|P(\varphi_T - A \bullet \varphi_E)\|_2^2\ +\ \lambda^2 \|L \bullet \varphi_E\|_2^2 \tag{3}$$

Where $\|\bullet\|_2$ indicates the Euclidean norm, matrix P represents the a priori knowledge of the measurements; φ_T the vector of the measured torso potentials; ϕ_E a vector of unknown epicardial potentials, A the patient-specific matrix, λ denotes the regularization parameter and matrix L describes the constraint matrix.

The regularization parameter is a user defined scalar value and it is critical to choose an appropriate value for achieving useful solutions. A commonly used method for this is the L-curve method. This method uses a parametric plot of the regularization objective function (second part of the equation) against the corresponding residual objective function (first part of the equation) for a wide range of regularization parameters (λ). When this curve is plotted on a log-log scale, it often has a characteristic L-shape, see Figure 3. The "corner" represents a value

of λ that assumes an ideal balance between the two components that are minimized in equation (3).[48]

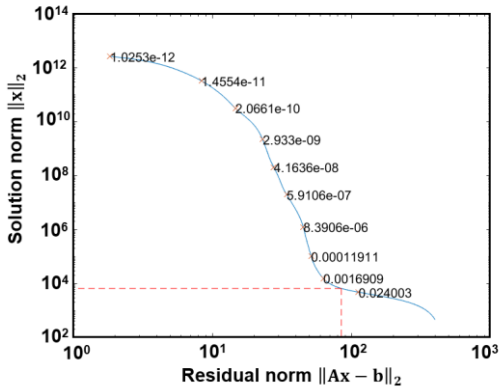

Figure 3 Example of the used L-curve method in ECGI for the reconstruction of epicardial unipolar electrograms

All methods have difficulties regarding the ill-posed inverse problem and reconstruction quality can heavily depend on parameter settings. It is important to realize that constraints are introduced purposefully to reach realistic solutions, but that this bias can create artefacts or prevent the reconstruction of electrical activity that is not accounted for in the constraints that were added.[38]

Finally, the reconstructed epicardial potentials can be visualized and analyzed in a three-dimensional (3D) plot of the ventricular epicardium.

1.5 Cardiac Magnetic Resonance

Cardiac magnetic resonance (CMR) can detect structural, functional, and tissue abnormalities of the cardiac muscle; in combination with other assessments, CMR can increase our ability to diagnose many diseases that affect the heart muscle that are most commonly associated with SCA. Alongside, LGE (both the presence and extent) in CMR has been found to be prognostic across a variety of cardiac diagnoses and clinical settings, including cardiac arrest survivors [49], [50]. CMR provides an additional role in determining the substrate for the ventricular arrhythmias in SCA survivors and for identifying those patients at risk of recurrent arrhythmias.[50] Patients can only be diagnosed with IVF after extensive testing. It is recommended to perform CMR in these patients. Since LGE became a routine sequence in CMR imaging in 1993, this is not performed in patients who are diagnosed with IVF before. In general, patients who are diagnosed with IVF show no abnormalities on CMR, but a small number of patients present LGE on CMR.

It is established that this can also be seen in healthy athletic individuals, which suggests that it can be of limited clinical significance [51]. On the other hand, a study revealed concealed pathologic substrates such as focal myocarditis or cardiomyopathy and conduction system diseases by a histologic study in young, SCA patients with an apparently normal heart (clinically unrecognizable). Corrado et al. analyzed 273 consecutive SCA cases < 35 years and found concealed pathologic changes by histologic examination in 22% of the study population. These findings may appear on CMR as presence of LGE.[52] Zhang et al. demonstrated that focal myocarditis with necrosis can be a possible contributing factor in cases of unexplained sudden death [53]. These results presume that small regions of LGE in IVF patients can contain information about the malignant arrhythmogenic substrate for development of VF.

An algorithm for calculating repolarization parameters

1 Introduction

The suspicion for the role of abnormalities in cardiac repolarization in patients with idiopathic ventricular fibrillation is elucidated in chapter 2. Therefore, we want to analyze repolarization patterns in this patient population using ECGI.

At the moment, the surface ECG is used to quantify repolarization abnormalities using different parameters and it has been stated that these parameters may be useful to predict malignant cardiac arrhythmias [7], [54], [55]. In this chapter, the development of an algorithm detecting different points of the T-wave in unipolar electrograms is described. At least the following repolarization parameters can be calculated using the defined points: Tpeak-Tend (Tp-e) interval, T-wave area, the amplitude of the T-wave and T-wave alternans. However, for the calculation of repolarization parameters, it is important that electrograms are free from noise, especially baseline wander. Therefore, an extra step is included in the algorithm from Maastricht, which will be described in the first section of this chapter [43]. This de-noising method leads to noise free body surface potentials and results in less noise in the reconstructed electrograms. In this way, the calculation of the repolarization parameters will become more reliable, since noise contains frequencies that can result in "waves" that can be recognized as T-wave peaks by the algorithm.

1.1 Tpeak-Tend interval

It has been demonstrated that the peak of the T-wave corresponds with the repolarization of epicardial cells and that the end of the T-wave represents the repolarization of the M-cells. From this point of view, the Tpeak-Tend (Tp-e) interval is considered as a measure for transmural dispersion of repolarization, defined as the difference in repolarization time between the M and epicardial cells. This parameter has been evaluated in several clinical conditions and seems to be useful to predict cardiac arrhythmias [22], [55], [56].

Various clinical conditions show a prolonged Tp-e interval. Letsas et al. investigated the interval in patients with ERP and found increased values of the interval in these patients compared to healthy individuals [57]. Patients with LQTS

show also a prolonged Tp-e interval according to several investigations.[58]–[60] This can offer incremental value for risk stratification in these patient populations. For example, Yamaguchi et al. evaluated the Tp-e interval in LQTS patients with and without TdP. The results show an interval of 185 $\pm$ 46 ms in patients with TdP and an interval of 84 $\pm$ 18 ms in patients without TdP, $P < 0.0001$ [61]. It is suggested that a long Tp-e interval is associated with more recurrence of life-threatening cardiac events in patients with BrS [62], [63]. Castro Hevia at al. established that BrS patients with Tp-e values $\geq$ 100 ms experienced events during 60 months follow-up. However, some investigators found no prolongation of Tp-e intervals in patients with Brs [64]. These outcomes suggest that the Tp-e interval distinguishes patients with IVF from healthy individuals.

1.2 T-wave area

Spatial dispersion of repolarization, measured with T-wave heterogeneity, appears to be predictive for impeding ventricular arrhythmias, such as ventricular tachycardia and VF, leading to SCA [65], [66]. Experimental studies on canine and rabbit hearts revealed that the value of the T-wave area correlates significantly with dispersion of action potential durations and dispersion of recovery times [46], [67]. In addition, it was demonstrated that T-wave area correlates linearly with dispersion of repolarization [68]. Kenttä et al. suggests that T-wave area acts as a non-invasive measured predictor of arrhythmia vulnerability [69]. These results indicate that the T-wave area may differ in patients with IVF compared to healthy individuals.

1.3 T-wave amplitude

The clinical significance of the T-wave amplitude is not reported in literature as far as we know. However, since the peaks of the T-wave and baseline are both calculated by the algorithm, it is an easy parameter for analysis. In the future, all details concerning depolarization and repolarization will be investigated to find possible parameters that correlate with the development of (idiopathic) VF.

1.4 T-wave alternans

T-wave alternans refers to a beat-to-beat alternation in the morphology and amplitude of the ST-segment or T-wave, what is due to a beat-to-beat alternation of action potential duration at the level of cardiac myocytes [70]. Over the last

years, this marker has emerged as a predictor of ventricular arrhythmias and sudden cardiac death [70]–[73]. The results indicate that this marker may play a significant role in risk stratification for patients with IVF and their relatives.

2 Methods for development

2.1 Filtering body surface potentials

By measuring body surface potentials, the depolarization and repolarization of the cardiac cycle is represented in a waveform. For example, propagation of activation through the His-Purkinje system and ventricular myocardium forms the fast-moving QRS complex, but repolarization spreads very slowly and forms the slow-deflecting T-wave, depicted in Figure 1. These differences in speed of wavefront propagation through the cardiac cycle are represented by different frequency contents of the typical ECG-waves. The content of the P-wave is characterized by 5-30 Hz frequencies, the QRS complex usually contains within 8-50 Hz and the T-wave frequency lays mostly up to 10 Hz.[74] The recording of body surface potentials in ECGI includes also different types of noise, such as powerline artifacts, motion artifacts and baseline wandering caused by e.g. respiration. Many approaches have been reported in the literature to reduce noise in body surface measurements, such as Empirical Mode Decomposition (EMD), infinite impulse response (IIR) filtering, finite impulse response (FIR) filtering, morphological filtering and wavelet filtering [75]–[78].

In this section, the method for the removal of noise based on wavelet filtering will be addressed. Three other methods for signal de-noising, including Butterworth band pass filtering, moving-median filtering and morphological filtering, were also applied to the signal and results were compared [79]–[81]. A detailed description of the other methods is given in Appendix I. Two requirements for baseline correction were formulated. First, it had to remove the low-frequency and high-frequency elements that are not related to the cardiac electrical activity and second, it was essential that the shape and amplitude of the PQRST complexes were preserved, especially the ST-segment is important because the repolarization of the heart cycle is of special interest in this thesis. Morphological filter and moving median filtering are both non-linear approaches. Therefore, we could not analyze the frequency responses of the filters. Instead of the frequency response, we used the amplitude spectrum using the Fast Fourier Transform (FFT) of the unfiltered and filtered

signals to choose the best method for noise removal. The amplitude spectrum of the original signal and filtered signals according to different methods can be seen in Figure 4. Since the frequency content of the characteristics of the heart cycle can be found up to 50 Hz, we are not interested in frequencies higher than this value. Furthermore, baseline wandering caused by respiration includes frequencies up to 0.5 Hz, thus frequencies smaller than this value have to be removed. [82] Figure 4 demonstrates that frequencies between 0.5 and 50 Hz are preserved optimally using wavelet filtering.

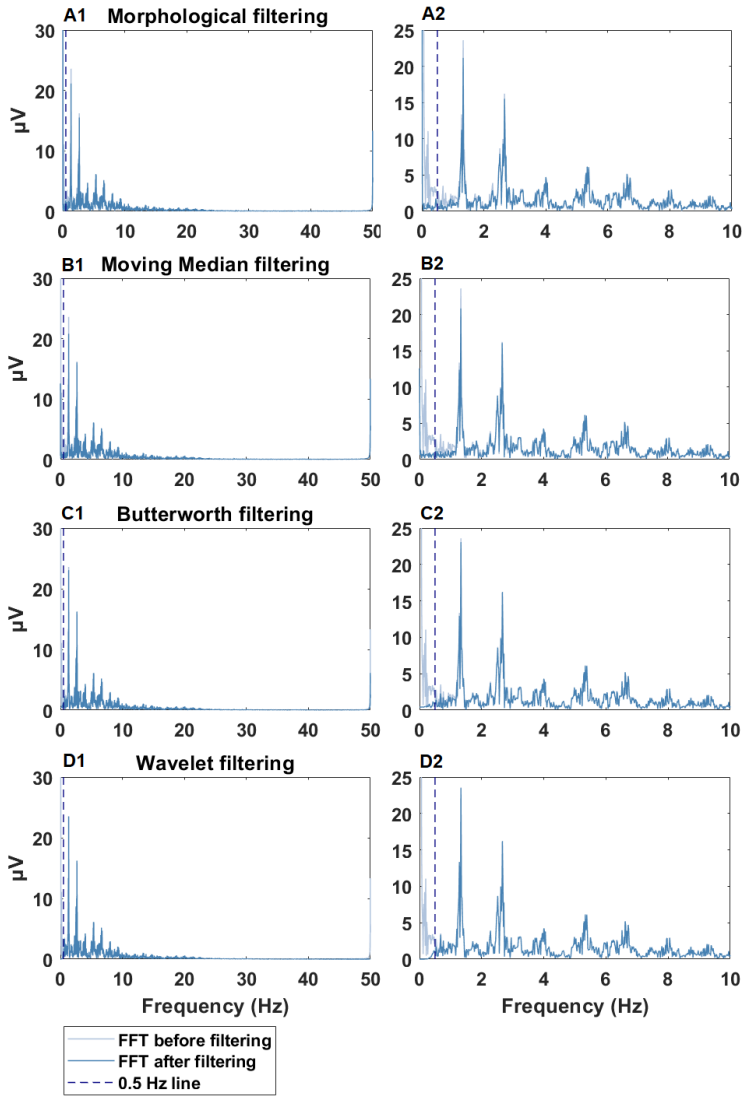

Figure 4 FFT of a signal of the original body surface measurement and after application of morphological filtering, moving median filtering, Butterworth band-pass filtering and wavelet filtering.

The wavelet transform

The Wavelet Transform (WT) has the ability to analyze transient, non-stationary signals, including the ECG. It provides a description of the signal in the time-scale domain and represents temporal features at different resolutions, according to their frequency content. Different types of noise and artifacts can be removed because of their different contribution at various scales.

The WT is a decomposition of the signal as a combination of a set of basis functions, obtained by means of dilation (a) and translation (b) of a single prototype wavelet $\boldsymbol{\psi}(t)$. The WT of a signal $x(t)$ is defined as:

$$WT_a[x(t)] = \frac{1}{\sqrt{\alpha}} \int_{-\infty}^{\infty} x(t) \bullet \boldsymbol{\psi} \left(\frac{t-b}{a} \right) dt \qquad (4)$$

The larger the scale factor a, the wider is the basis function, which gives information about the lower-frequency components of the signal and vice versa. The WT has high temporal resolution at high frequencies and low temporal resolution at low frequencies and achieves the time-frequency decomposition of signal $x(t)$.

In biomedical signal processing, the Discrete Wavelet Transform (DWT) is often used as a method in for example signal de-noising, detection of abrupt discontinuities and compression of large amounts of data. The DWT has the ability to characterize simultaneously a signal in time and frequency domain. A schematic overview of signal decomposition by DWT up to level three is depicted in Figure 5A. In practice, the DWT of a signal $x(n)$, with N the number of samples, is calculated by passing it through a low-pass filter. This gives the low frequency components, that are also known as approximation coefficients (cA) with N/2 samples, which means that the length is halved. Next to that, the signal is passed through a high-pass filter. This gives the high-frequency components, that are also known as detail coefficients (cD) with N/2 samples. This process is repeated over the approximation coefficients by increasing the level of decomposition. At each level, the signal is being downsampled by a factor two resulting in halving the length of the signal. This decomposition process is carried out until the required frequency is achieved from the given input signal.

The main disadvantage is the decreasing length of the coefficient sequences with the increase of the level due to the use of the decimators. This can lead to loss of

the original resolution of the signal, which can lead to a more difficult and less precise identification of characteristic points. To overcome this problem, the Stationary Wavelet Transform (SWT) can be used.[75]

Stationary wavelet transform

Unlike DWT, SWT does not incorporate down sampling operations. In this way, the length of both coefficient sequences, cA and cD, have the same length as the input signal, at each level. This multiresolution in the SWT is achieved by upsampling the two coefficients of the low pass and high pass filter by a factor of two, at each level of decomposition. A schematic overview of signal decomposition by SWT up to level three is depicted in Figure 5B.

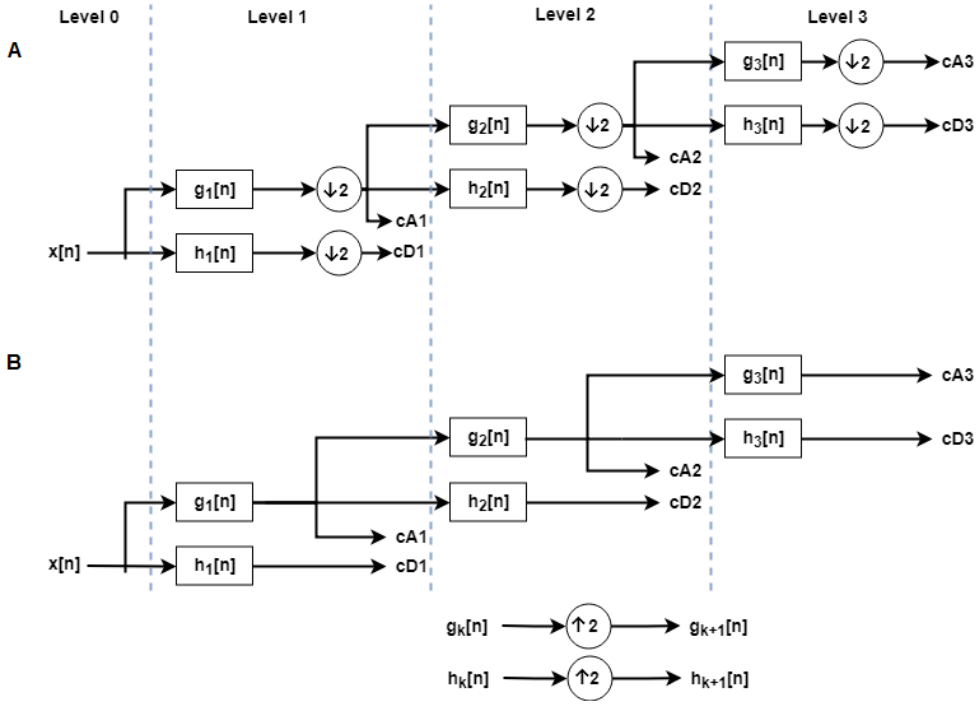

Figure 5 The scheme of the system that computes the stationary wavelet transform. The systems with the impulse responses h_k are low-pass filters and the systems with impulse responses g_k are high pass filters. Figure modified from [76]

Signal de-noising

For signal de-noising, components that are not related to the cardiac cycle have to be removed. Two dominant artifacts are baseline wander, that is due to respiration or the motion of the patient or the instruments, and high-frequency

noise caused by electromyogram induced noise, powerline interferences or mechanical forces acting on the electrode [77].

Since the SWT has the ability to decompose the signal in low- and high-frequency components at different scales, both baseline wander and high-frequency noise can be isolated by this method. The estimation of the baseline wander is realized by high-pass filtering, since this type of noise is caused by low-frequency components. To do this, the SWT of the measured body surface potentials is computed, using K decomposition levels. Next, all approximation coefficients are set to zero. Subsequently, the inverse SWT, ISWT of the new sequence is computed and the signal that is free from baseline wander is obtained.

The same method is used to eliminate high frequencies in the measures body surface potentials, although this is realized by low-pass filtering and therefore the detail coefficients are set to zero to obtain the noise-free signal.

Decision parameters used in the proposed method

Wavelet choice

There is no absolute rule for the choice of wavelets, but it is recommended to choose a wavelet function that corresponds closely to the processed signal. In this work, the Daubechies 4 (db4) wavelet is chosen, because of its similar shape of the ECG. It has been stated that this wavelet is suitable for de-noising ECG signals [83].

Level decomposition choice

The measured body surface potentials contain different types of noise with different frequency contents. The selection of the decomposition level is important for proper removal of baseline wandering and high-frequency noise. The removal of noise can be achieved by setting the coefficients at corresponding frequency bands to zero. The required decomposition level to achieve a cut-off frequency f_c depending on the sampling frequency f_s can be given by [84]:

$$L = log_2\left(\frac{f_s}{f_c}\right) - 1 \qquad (5)$$

First, baseline wandering, caused by low-frequency components, has to be removed. A cut-off frequency of 0.5 Hz is chosen for this, which means that the 11th scale, based on equation (5), is chosen for removal of baseline wandering. The

frequency response in Figure 6A demonstrates that level 11 is appropriate for this. Since the frequency content of important information of the heart cycle is up to 50 Hz, this cut-off frequency is chosen for the removal of high frequencies [74]. The 5th scale corresponds to this cut-off frequency according to equation (5). Figure 6B indicates the suitability of this level for the high-frequency removal.

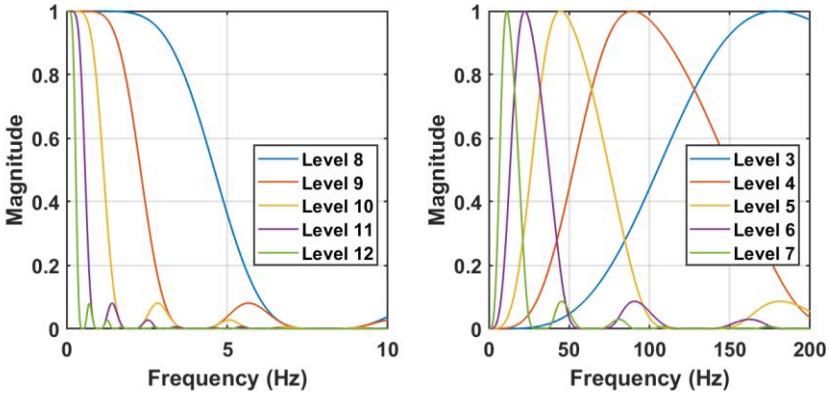

Figure 6 Frequency responses of different levels of (A) the approximation coefficients and (B) the detail coefficients corresponding to the Daubechies 4 wavelet.

An example of the removal of baseline wander and high-frequency noise can be seen in Figure 7.

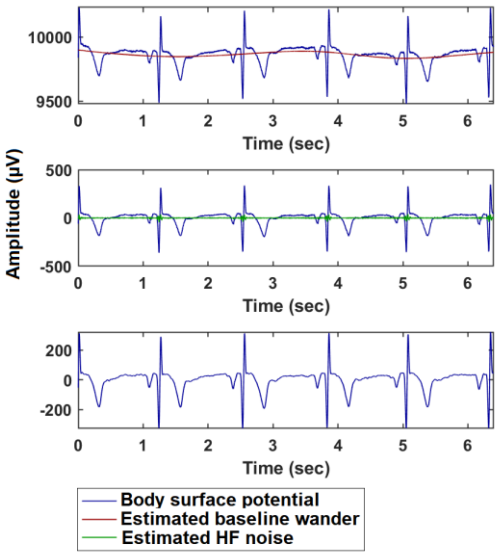

Figure 7 An example of removal of baseline wander and high-frequency noise in a body surface potential measurement. The first plot respresents the estimated baseline and the second plot the estimated high frequency noise. The third plot shows the noise-free signal obatined by wavelet filtering.

2.2 T-peak detection

In this section, the algorithm for T-wave detection is described. First, a method for smoothing the electrograms is proposed. Subsequently, the method for determination of the isoelectric line is suggested and finally, a detailed description for the detection of the peaks and the end point of the T-wave is given.

Signal pre-processing

The reconstructed electrograms contain high frequency noise and this makes it difficult to detect the different points in the T-wave. Since the frequency content of the T-wave is up to 10 Hz, it was decided to filter the signal with a Savitzky-Golay filter [74]. This filter is known as a finite impulse response (FIR) smoothing filter for the purpose of removing or smoothing noise from a wideband noisy signal. A polynomial function is fit to a signal piece-by-piece with the least-squares method and the original values are replaced with smoothed values. For Savitzky-Golay filtering, it is important to choose an appropriate window, i.e. the correct number of data points to be used for fitting in order to preserve the valid information, but discard noise.[85], [86] Based on the frequency content of the T-wave of 10 Hz and the frequency responses in Figure 8 a polynomial order of 2 and a window length of 199 is chosen for signal smoothing.

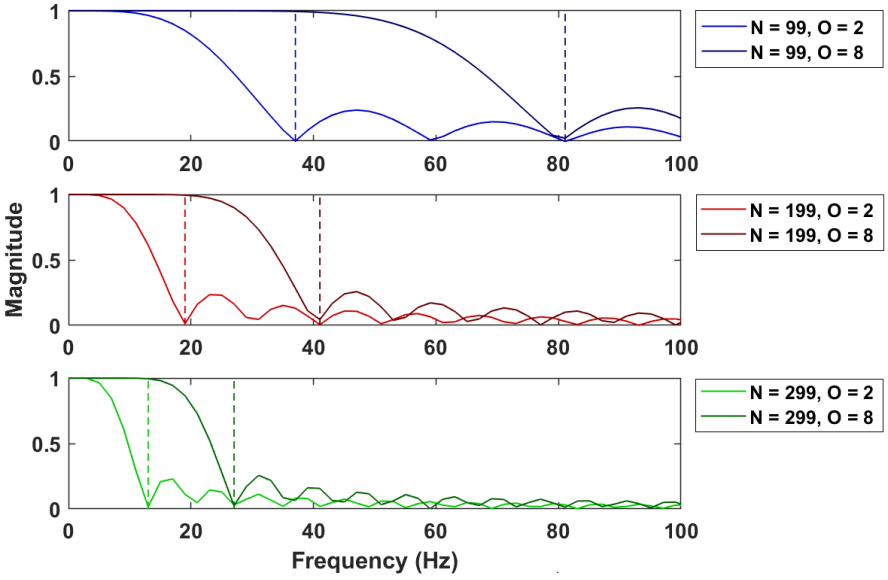

Figure 8 Frequency responses of the Savitzky-Golay filter using different window lengths and orders.

Determination of the baseline

According to the AHA/ACCF/HRS Recommendations for the standardization and interpretation of the electrocardiogram, the isoelectric line was taken as the TP-segment and calculated as the mean from the beginning of the electrogram until the start of the P-wave and from the end of the T-wave until the end of the signal (see Figure 1)[87].

2.3 Method for T-wave detection

The method for T-wave detection developed in this study consists of four different parts. First, a method proposed by Cesari et al. is applied to the electrograms for defining candidate monophasic and biphasic T-waves [88]. After this, an in-house developed method, based on maxima, minima and derivatives is implemented for the detection of the T-wave. Subsequently, both methods are compared and the final monophasic and biphasic T-waves are chosen based on the mean derivative around the detected T-peaks. Eventually, neighboring signals, localized on the three-dimensional (3D) mesh, are compared which makes us able to change the index of wrong detected T-waves.

Method 1: A wavelet-based detection algorithm

For T-wave detection, we have developed an algorithm that takes inspiration from the work of Cesari et al. but a few changes are made [88].

First, we decided to apply the Daubechies 4 (db4) mother wavelet. The frequency response for different levels of the mother wavelet can be seen in Figure 9 for a sampling frequency of 2048 Hz. It was chosen to consider the 7^{th} scale of the WT (labelled as $WT7$) for T-peak detection because its frequency band fits the frequency content of the T-wave. Next to that, the window for the T-wave is manually defined by the user.

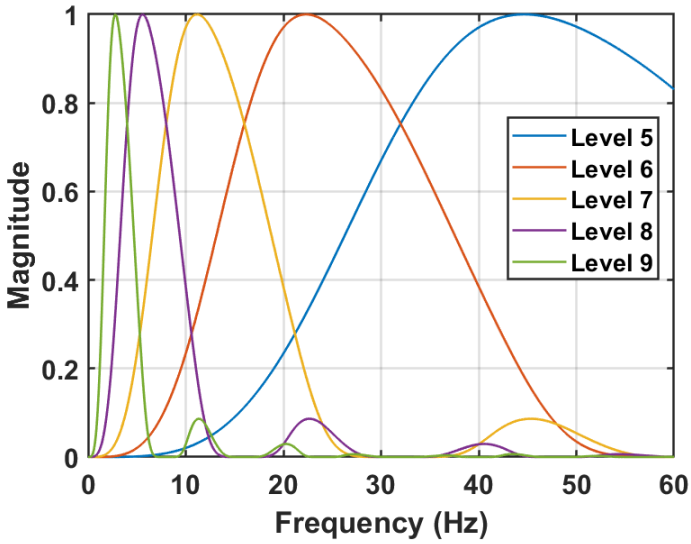

Figure 9 Frequency response of the SWT of the Daubechies 4 wavelet from different level for a sampling frequency of 2048 Hz.

The steps for detecting the peaks of the T-wave are listed below [88]:

1. The searching window for the T-wave is defined as the interval from 50 ms after the start of the ST-segment until the end of the ST-segment (see Figure 10A).
2. For each signal, the positive (P) and negative (N) peaks of the $WT7$ are found within the window.
3. The mean of the positive peaks (m_p) and negative peaks (m_n) are calculated. The positive peaks having an amplitude lower than $0.4 \times m_p$ and the negative peaks having an amplitude larger than $0.3 \times m_n$ are removed because of their low amplitude.
4. For each signal, all zero-crossings, z, of the $WT7$ are detected in the T-wave window.
5. The pairs of positive and negative peaks that are closer than 200 ms are found. This is done because a T-wave is defined by a positive and negative slope. Next to that, the maximum duration of the T-wave is 200 ms.
6. Each pair of peaks is then analyzed. If the positive peak P precedes the negative peak N, a positive T-wave is expected. All zero-crossings, z, between P and N are considered. The zero-crossing in correspondence with the highest ECG value is labeled as z. Subsequently, the maximum value of the ECG in a window of 30 ms around z is chosen as the candidate T-peak.

In case of a positive peak following a negative one, a negative T-wave is expected and thus, the lowest ECG value is searched. An example is given in Figure 10B.

7. For each pair of peaks, the following index is calculated:

$$S = 1.5\ |WT7\ N\ | + 1.5\ |WT7\ P\ | + |C_{Ti}|$$

The candidate T-peak with the highest value for S is defined as the primary T-peak (S_p). From Figure 10B, it can be seen that the second window represents the primary T-peak, according to the formulated criteria.

8. Finally, a check for possible presence of biphasic T-waves is performed. If the primary T-wave is positive, the secondary lobe of a biphasic T-wave is negative and it may occur either before or after the primary lobe. For this reason, the pairs of peaks of the *WT7* for identifying the primary T-peak can be used to find biphasic T-waves and are therefore analyzed again. To do this, the pairs of the *WT7* peaks having in common one peak of the ones used for identifying the primary T-peak, are analyzed. For each of these pairs, the candidate secondary T-peak is found and the value of S is calculated in the same way described before. The candidate secondary T-peak having the highest value is chosen and is labelled as S_s. If $S_s > 0.6 \times S_p$, the T-wave is considered biphasic and it is characterized by the primary and secondary T-peaks, otherwise the primary T-peak constitutes the T-peak of a monophasic T-wave.

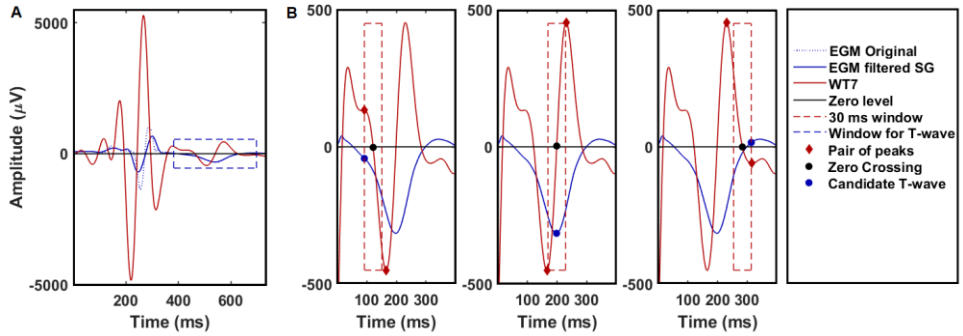

Figure 10 An example of the peak detection by the wavelet method proposed by Cesari et al. [88] (A) Selection of the window where the peak of the T-wave is expected. (B) An example of the primary T-peak in a window. The pairs of peaks od the WT are considered and the zero crossing z between them is used to identify the candidate T-peak in a 30 ms window.

Method 2: A detection algorithm using wave characteristics

Next to the wavelet method, another method for T-peak detection is developed. This method is based on features of the ECG and the steps in this method are included a flowchart, see Figure 12.

The steps for detecting the peaks of the T-wave are listed below:

1. The amplitude of the QRS complex for each signal is found by defining the maximum and minimum value within the QRS segment. The QRS segment is defined manually by the user by clicking. The largest absolute value from these two points is taken as the QRS-amplitude.
2. For each signal, the maximum and minimum value within the ST-segment are found. However, the window for the ST-segment is adapted. It is assumed that the (first) peak of the T-wave is located at least 100 ms after the QRS complex, so therefore the ST-segment starts 100 ms later compared to the wavelet method.
3. The T-peak is labelled as positive when the value of the maximum exceeds the value of $0.2 \times$ absolute QRS amplitude. The T-peak is labelled as negative when the value of the absolute minimum is lower than $0.2 \times$ absolute QRS amplitude. When the maximum and the minimum are both lower than $0.2 \times$ absolute QRS amplitude, the T-peak is labelled as a flat T-wave and both minimum and maximum are included.
4. Candidate T-peaks are considered as biphasic in the case of two detected peaks. In case of only one detected T-peak, the T-wave is labeled as a candidate monophasic T-wave and a check for a possible biphasic T-wave is performed in step 5.
5. The second peak of the biphasic T-wave can be found either before or after the primary T-peak. For this reason, the maximum and minimum value of the derivative are searched within a window of 150 ms before and after the primary T-peak. This window is chosen because the length of the T-wave should not exceed 200 ms [89]. In case of a positive, primary T-peak, it is expected that the index of the minimum derivative is located before the index of the maximum derivative, and the opposite is expected for a negative, primary T-peak. The T-wave is considered biphasic when both the minimum and maximum derivative have an absolute value that exceeds 0.3. If the maximum and minimum derivatives before and after the primary T-wave exceed the value, the peak with the highest absolute value is

considered as the second peak of the T-wave. The value 0.3 is chosen arbitrary after testing.

6. If one of the derivatives before and after the primary T-wave do not satisfy the criterion, the T-wave is considered as monophasic.

2.4 Define final T-peak

The T-peaks determined by both methods are analyzed in order define the final decision for the T-peak.

First, the mean gradient in a window of 50 ms before and after the primary, and, if present, the secondary, is calculated. Next to that, the overall absolute mean gradient, thus the over the gradient before and after the primary and secondary T-peak is calculated. The T-wave with the highest mean derivative around the T-peak is selected as the final T-peak. When for one of the two methods, the derivatives before as well as after the T-peak are larger or smaller than zero, the T-peak defined by that method is discarded. An example is given in Figure 11. The orange triangle inidcates the T-peak calculated with the Wave characteristics method, the red dot depicts the T-peak calculated according to the Wavelet method. The calculated absolute mean value of the gradient in 50 ms before and after the T-peak is larger for the Wavelet method T-peak; 0.42 compared to 0.36. However, the mean value before and after the peak have a value larger than zero; -0.43 in the 50 ms window before the peak and -0.40 in the 50 ms window after the peak. Based on these criteria, the T-peak calculated with the Wave characteristics method (orange triangle) is chosen as the final primary T-peak.

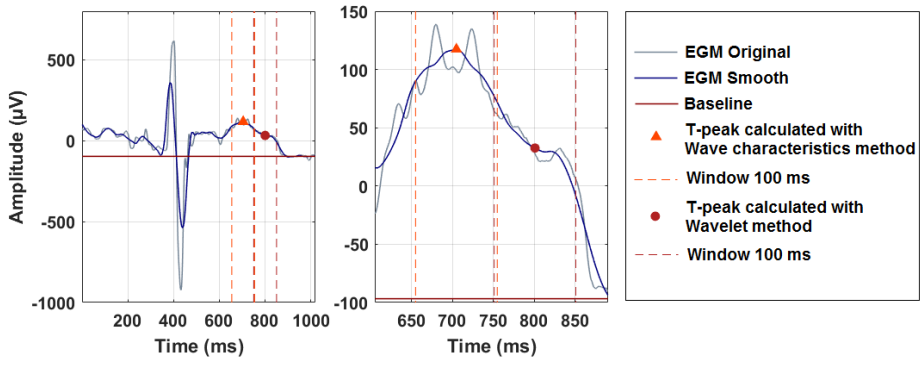

Figure 11 Example of method for determination of the final T-peakbetween the two proposed methods, using the gradient in a window of 50 ms around the calculated T-peaks.

Finally, biphasic T-waves are analyzed. The ratio between the mean derivatives is calculated. When the mean derivative of the primary peak is larger than the mean derivative of the secondary peak, the ratio is calculated as the mean derivative of the primary peak divided by the mean derivative of the secondary peak. In case of a larger mean derivative of the secondary peak, compared to the mean derivative of the primary peak, the ratio is calculated as the mean derivative of the secondary peak divided by the mean derivative of the primary peak. Secondary peaks are removed when the ratio has a value smaller than the arbitrary chosen value of 0.6. T-waves are considered as biphasic when de ratio has a value larger than 0.8. When the value of the ratio is larger than 0.6, but smaller than 0.8; an additional parameter is calculated: the ratio between the absolute amplitudes of the primary and secondary peak, defined as the difference between the height of the peak and the baseline. The T-wave is considered as biphasic when this ratio exceeds the arbitrary chosen value of 0.15, otherwise the peak with the largest absolute value is considered as the primary, monophasic peak.

2.5 Check neighboring signals

Finally, a check on the T-peaks is performed by taking neighboring signals into account. If we are looking to the mesh of the three-dimensional (3D) plot Figure 13, the mesh consists of triangles. Each vertex of a triangle corresponds to one of the reconstructed electrograms. Similarities between signals are approximated by the calculation of the correlation coefficients over the ST-segments between the vertices. Furthermore, the correspondence between the identified T-peaks for each triangle is determined. It is assumed that T-peaks correspond when the indices are closer than 30 ms. When the correlation coefficients between vertices are highest between two signals, but the T-peaks do not correspond, the peaks of the T-wave can be manually adapted. When indices of T-peaks within the window do correspond in de triangles, it is assumed that the peaks are correctly identified.

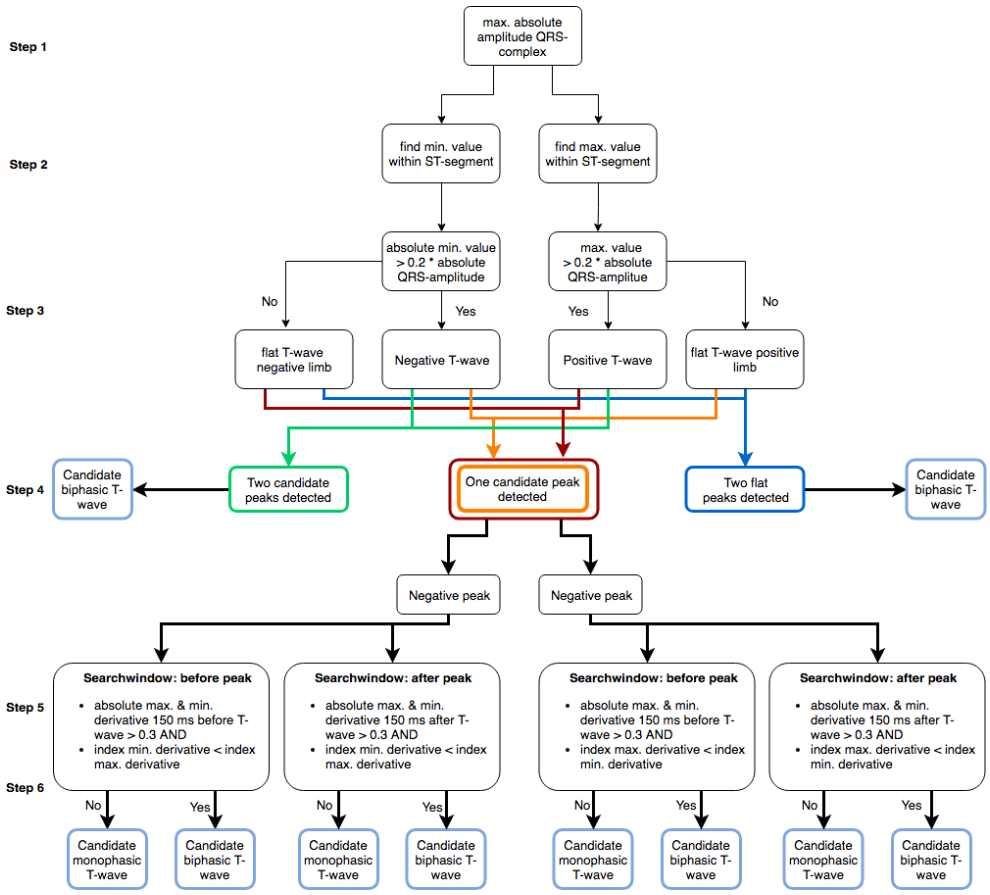

Figure 12 Flowchart of the included steps in the second method used for peak detection in the T-wave, based on wave characteristics.

2.6 T-wave end

Different methods for the determination of the end of the T-wave are included in the algorithm since there is no definition for the determination of the end of the T-wave in ECGI. Interpretation of the T-wave morphology on body surface ECGs might be different from that on local electrograms reconstructed by ECGI [90].

The first method for the determination of the end of the T-wave is commonly used in the clinical setting for the evaluation of the ECG and assessed in reports in literature. In this method, also called the “tangent method”, the end of the T-wave is defined as the intersection of a tangent to the steepest slope after the last T-peak of the T-wave and the baseline.[91]–[93]

An alternative for this method is proposed by Erikssen et al. and Sallas et al. This method is called the “tail method” and defines the end of the T-wave as the time where the signal after the peak of the T-wave reaches the baseline for the first time [77], [94].

2.7 Check for T-wave points

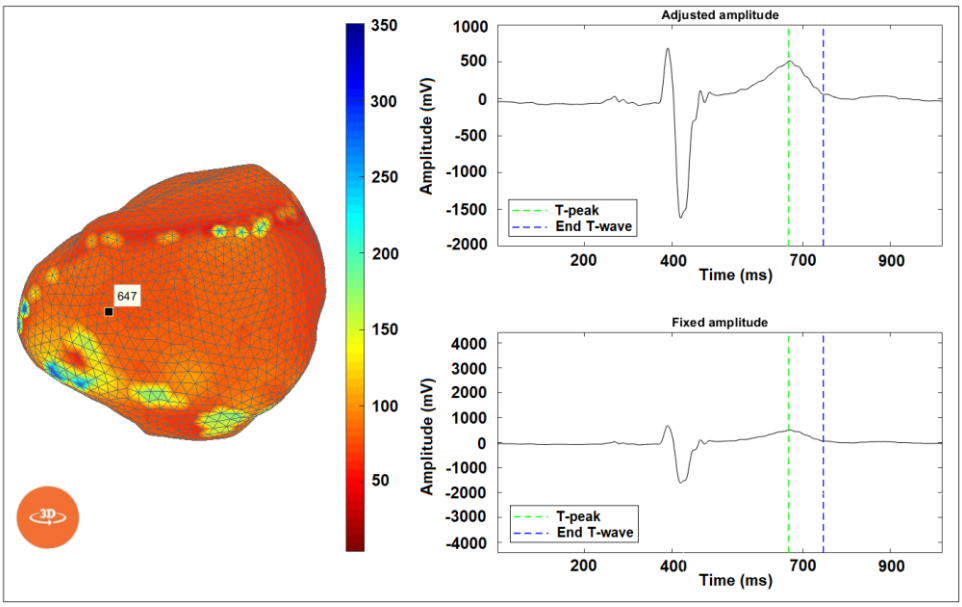

Figure 13 An example of the visualization tool of the epicardial unipolar electrograms reconstructed with ECGI. T-wave points calculated by the algorithm can be depicted in the electrogram plots.

A MATLAB tool is developed to check whether the algorithm detects the points in the T-wave correctly. An example is depicted in Figure 13. The user can click on the points in the epicardial mesh and de corresponding electrogram with the detected points will be displayed. This enables the user to verify (ab)normal areas of repolarization parameters.

2.8 Validation

To assess the performance of the T-wave detection algorithm, the difference between automatic and manual annotations are evaluated. As there is no database available including reconstructed unipolar electrograms by ECGI, the validation of the algorithm is performed by using manually annotated databases. For this purpose, two PhD students of the department of Cardiology in the UMCU were asked to annotate the peak(s) of the T-wave (one peak in case of a monophasic T-wave, two peaks in case of a biphasic T-wave) and the end of the T-wave.

The Association for the Advancement of Medical Instrumentation (AAMI) recommends the following measures for evaluation: 1) Sensitivity, $Se = \frac{TP}{TP+FN}$, 2) Positive Predictive Value, $PPV = \frac{TP}{TP+FP}$, 3) False Positive Rate, $FPR = \frac{FP}{TN+FP}$ and 4) Overall accuracy, $Acc = \frac{TN+TP}{TN+TP+FN+FP}$, where TP is the number of true positive detections, TN stands for the number of false negative detections, FP

gives the number of false positive misdetections and *FN* the number of false negative detections. Sensitivity and the Positive Predictive Value are also known in literature as recall and precision, respectively.[95] Furthermore, the average of the errors, m, is calculated as the time differences between automatic annotations by the algorithm and manually annotated points by the PhD students. The signal s corresponds to the standard deviations of the errors. Agreement indicates the percentage cases where both observers annotated points within the tolerances regarding each other.

3 Testing and results

3.1 Validation

Table 1 The performance of the algorithm with respect to observer 1 and 2 and the inter-observer difference.

Observer	**Parameters**	**Prim. T-peak**	**Sec. T-peak**	**T-end**
Observer 1	# Annotations	200	24	200
	TP	151	4	24
	TN	0	174	0
	FP	0	2	0
	FN	49	20	176
	SE (%)	75.5	16.7	12.0
	PPV (%)	100	67.5	100
	FPR (%)	N/A	9.1	N/A
	Acc (%)	75.5	89.0	12.0
	%Error	24.5	91.7	88.0
	m ± s (ms)	-15.5 ± 42.4	0 ± 0.1	-105.5 ± 114.8
Observer 2	# Annotations	200	38	200
	TP	187	5	55
	TN	0	161	0
	FP	0	3	0
	FN	13	33	145
	SE (%)	93.5	13.2	27.5
	PPV (%)	100	62.5	100
	FPR (%)	N/A	1.1	N/A
	Acc (%)	93.5	82.7	27.5
	%Error	6.5	89.5	72.5
	m ± s (ms)	-23.9 ± 33.2	0 ± 0.2	-33.2 ± 55.3
Observer 1 vs observer 2	Agreement (%)	73	73*	26
	m ± s (ms)	8.3 ± 36.2	0 ± 0.2	-72.3 ± 137.6
	Tolerances (ms)	27.8 (2s)[96]	27.8 (2s)[96]	30.6 (2s)[97]

(*) = In total, observer 1 annotates 24 biphasic T-waves and observer 2 annotates 38 biphasic T-waves. From these biphasic T-waves, a total of 15 are annotated in the same signal. Observer 1 and 2 agree in 11 cases.

In table 1, the performances of the algorithm with respect to the observers and the inter-observer difference are shown. The last row of the table shows the accepted two-standard-deviation tolerances proposed by Martinez et al. and the CSE Working Party [96], [97].

Repolarization patterns in patients with idiopathic ventricular fibrillation using non-invasive electrocardiographic-imaging

1 Introduction

This chapter includes the analysis of repolarization parameters using ECGI in five IVF patients and one control subject. First, the study population and repolarization parameters are described. Subsequently, the results from the control subject are described in detail. Repolarization patterns of IVF patients are compared to the data of the control subject.

2 Methods

2.1 Study population

The proposed method is applied to ECGI-data of five patients diagnosed with idiopathic ventricular fibrillation and one control subject. The frequency of ICD therapy in all patients is listed in Table 2. In one IVF patient, ECGI was performed before and during quinidine treatment. Quinidine is a pharmaceutical agent that acts as a class I antiarrhythmic agent in the heart. It causes an increased action potential and a prolonged QT-interval.

Table 2 Frequency of ICD therapy of the patients analyzed in this study

Patient	ICD	Frequency ICD therapy
1	Yes	2
2	Yes	1
3	Yes	2
4	Yes	0
5	Yes	0

2.2 Data analysis

The data was obtained from the Maastricht University Medical Center (MUMC). The dataset contained the measured body surface potentials, the transfer matrix and the heart surface geometry.

For data analysis, six consecutive beats are selected from the measured body surface potentials. The QRS-complex and the ST-segment are selected manually for each beat. The selected beats and the transfer matrix served as input for the ECGI methodology for calculation of approximately 2000 epicardial potentials for each subject. After this, the proposed method for T-peak and T-end calculation is applied and the results are used for calculating various repolarization parameters.

Repolarization parameters

At the moment, ECGI is mainly used for analyzing activation and recovery times, but other parameters can be calculated from the reconstructed epicardial electrograms. These parameters may provide additional information about the electrical activity in the heart. Four different parameters are proposed in this thesis: the amplitude of the T-wave, Tpeak-Tend interval, T-wave area and T-wave alternans (see figure 14).

Amplitude

The amplitude of the T-wave is calculated as the difference between the height of the peak of the T-wave and the baseline. In case of a biphasic T-wave, the peak with the highest absolute amplitude value is considered as the amplitude. The algorithm calculates both positive and negative amplitudes, but the absolute value of the amplitudes can also be analyzed.

Tpeak-Tend interval

The Tpeak-Tend interval is calculated in different ways since monophasic and biphasic T-waves are considered in this study. In a biphasic T-wave, three different peak-types are considered. First, the peak at the first nadir of the T-wave. Second, the peak at the second (last) nadir of the T-wave. Finally, the peak with the highest absolute amplitude is considered as a peak type. For analysis, the end of the T-wave was defined as the point calculated by the tangent method: the point where the tangent of the after the last T-peak intersects the baseline [98]. From this point, three different Tp-e intervals regarding biphasic T-waves are calculated by the algorithm:

1. Tpeak-Tend first → In case of a biphasic T-wave, the interval between the first T-peak and the end of the T-wave is calculated

2. Tpeak-Tend last → In case of a biphasic T-wave, the interval between the last T-peak and the end of the T-wave is calculated
3. Tpeak-Tend highest amplitude → In case of a biphasic T-wave, the interval between the T-peak with the highest absolute amplitude and the end of the T-wave is calculated

In this thesis, the Tpeak-Tend first interval is used for analysis, since the first T-peak does not depend on the baseline. This method was also proposed by Antzelevitch et al. [62]

T-wave area

The T-wave area is defined as the absolute area between the electrogram and the baseline over the interval between the QRS-offset and the intersection of the signal with the baseline ("tail method"). This method has the advantage taking the terminal part of the T-wave into consideration. Erikksen et al. states that the terminal part of the T-wave may be of prognostic importance, especially in acute myocardial infarction. He investigated the prognostic value of Tp-e measured according to the tail method and the traditional tangent method as a predictor of mortality during the first year after acute myocardial infarction, and demonstrated that Tp-e measured according to the tail method was a better prognostic instrument in this case. [94]

T-wave alternans

In this thesis, T-wave alternans is defined as the difference in amplitude of the primary T-peaks between the reconstructed epicardial potentials of two consecutive heartbeats. For all subjects, six consecutive beats were analyzed resulting in five approximations of alternans; amplitude difference between beat 1 and 2, beat 2 and 3, beat 3 and 4, beat 4 and 5, beat 5 and 6.

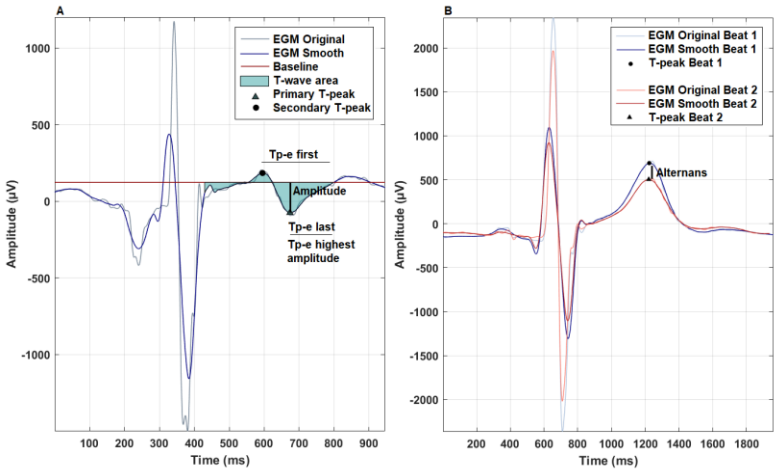

Figure 14 Example of different repolarization parameters proposed in this thesis.

3 Results

3.1 Control subject

Amplitude

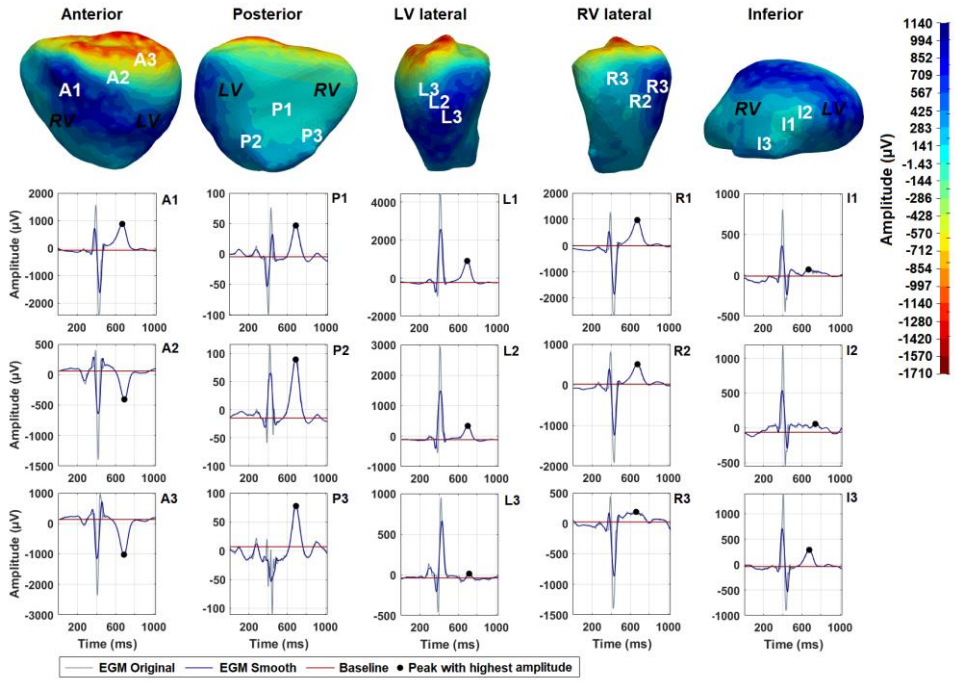

Figure 15 Epicardial amplitude maps of a control subject, reconstructed with ECGI. The left panel shows the 3D epicardial surface of the left ventricle (LV) and right ventricle (RV) from the anterior, posterior, left and right lateral and inferior view. The right panel shows the electrograms that correspond to the marked areas in the left panel. Example; electrogram A1 is localized in the "A1" marked area in the anterior view.

Figure 15 shows the T-wave amplitude of the epicardial potentials of a control subject during sinus rhythm. The superior part of the ventricles presents negative T-waves. A smooth transition to positive T-waves can be seen towards the inferior part of the ventricles. This transition occurs in a shorter area interval in the right ventricle (RV) compared to the left ventricle (LV). The posterior part of the ventricles shows a homogeneous area of negative T-waves that change into positive T-waves at the lateral part ventricles. The left lateral side of the ventricle demonstrates a smooth transition from negative T-waves into positive T-waves from the posterior part towards the anterior part of the LV. In general, the T-waves of the lateral side of the RV have a lower amplitude compared to the LV. The inferior part shows quite flat T-waves, especially in the region of EGM I1 and I2. Figure 15 does not show any abrupt changes in the amplitude of the T-wave in this control subject.

T-wave area

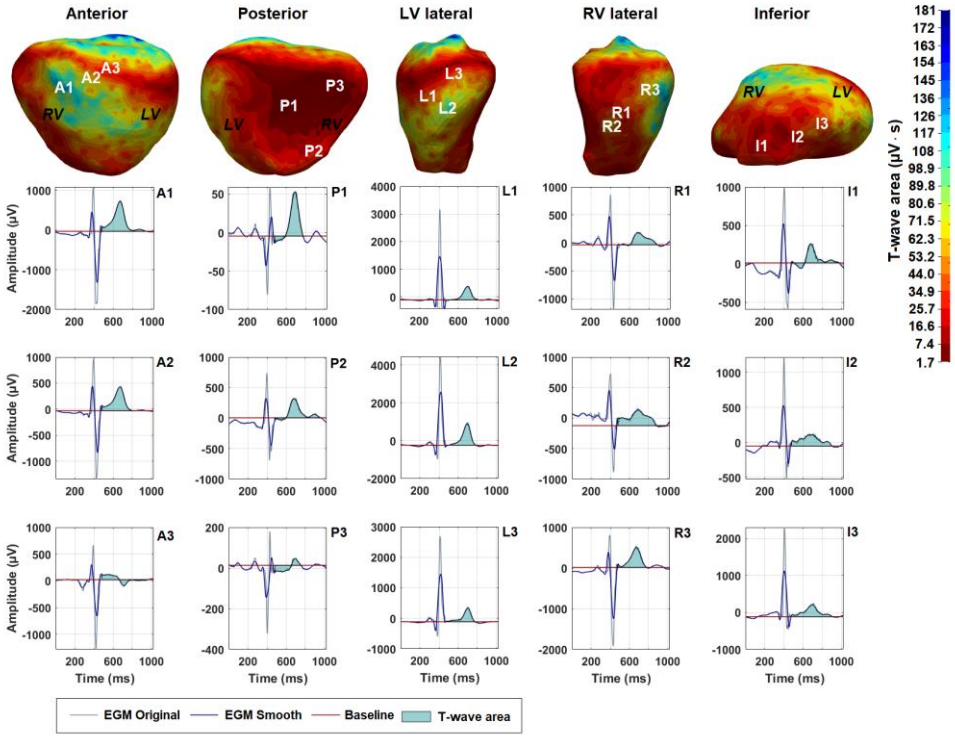

Figure 16 Epicardial T-wave area maps of a control subject, reconstructed with ECGI. The left panel shows the 3D epicardial surface of the left ventricle (LV) and right ventricle (RV) from the anterior, posterior, left and right lateral and inferior view. The right panel shows the electrograms that correspond to the marked areas in the left panel. Example; electrogram A1 is localized in the "A1" marked area in the anterior view.

The area of the T-waves of the epicardial potentials from a control subject are depicted in Figure 16. Regions with high positive amplitudes and low negative amplitudes show higher T-wave areas. From the posterior part, smaller T-waves are present in the center and become larger towards the borders of the ventricles. The left lateral side show higher T-wave areas compared to the right lateral side, which is corresponds to the T-wave amplitudes in Figure 15. It is remarkable that a small region with a larger area can be seen in R2, compared to the surrounded area. This region cannot be distinguished in the right lateral side in Figure 15. The amplitude of the T-wave in R2 is around 70 µV higher than R1. No abrupt changes in T-wave area are present in Figure 16.

Tpeak-Tend interval

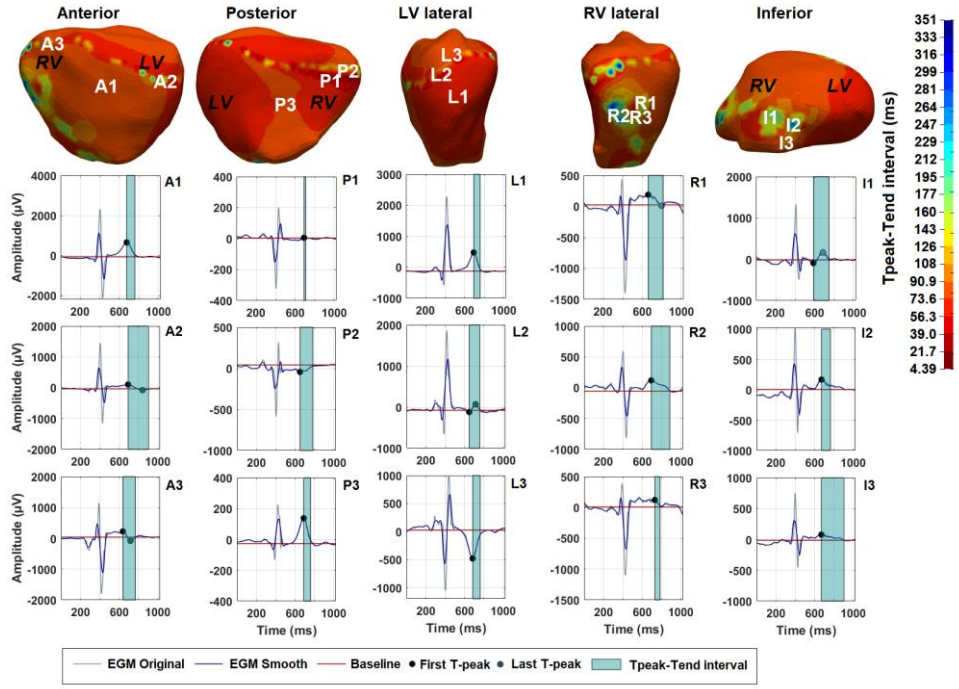

Figure 17 Epicardial Tpeak-Tend interval maps of a control subject, reconstructed with ECGI. The left panel shows the 3D epicardial surface of the left ventricle (LV) and right ventricle (RV) from the anterior, posterior, left and right lateral and inferior view. The right panel shows the electrograms that correspond to the marked areas in the left panel. Example; electrogram A1 is localized in the "A1" marked area in the anterior view.

Figure 17 shows the 3D plot of the epicardial Tpeak-Ted interval from the first peak of the T-wave till the end of the T-wave of a control subject.

The anterior part of the ventricles represents a uniform area with Tpeak-Tend intervals between 73.6 and 90.9 ms, but several distinctive areas can also be seen, for example in A2 and A3 which contain biphasic and flat T-waves. This distinctive

region continues toward the posterior part of the epicardium (P1 and P2. The main posterior part of the epicardium depicts a homogeneous surface indicating a nearly constant Tp-e interval. The left lateral side establishes the transition from negative (L3) to positive (L1) T-waves by a biphasic T-waves such as L2. The Tp-e interval is prolonged for the biphasic T-waves. Areas with a dissimilar Tp-e interval are remarkable on the right lateral part of the RV. Each of the electrograms R1, R2 and R3 represent a different interval.

T-wave alternans

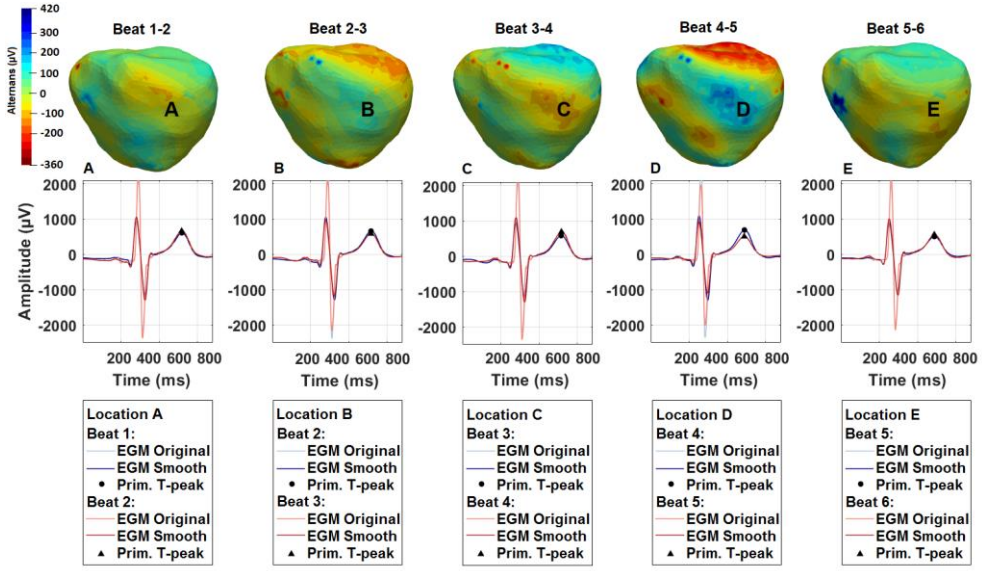

Figure 18 Epicardial T-wave alternans maps of a control subject, reconstructed with ECGI. The difference in T-peak amplitude is calculated for six consecutive beats. The letters A - E indicate the location of the epicardial electrogram. This location is equal for each heartbeat. The horizontal, central plane shows the electrograms for each set of beats.

Figure 16 shows the 3D plots of the epicardial T-wave alternans calculated over six consecutive heartbeats. Each 3D plot shows the alternans between two consecutive heartbeats. The letters A, B, C, D and E indicate the location of the electrograms depicted in the horizontal, central plane. The electrograms show minimal changes in T-wave morphology over time. The difference in amplitude for each set of beats amounts A: -49 µV; B: +75 µV; C: -105 µV; D: +186 µV; E: -54 µV.

3.2 Patients with idiopathic ventricular fibrillation

Since the T-wave area and the absolute value of the amplitude area linearly correlated, depicted in Appendix I Figure 24 , only the amplitude, the Tpeak-Tend interval and T-wave alternans are analyzed in these patients.

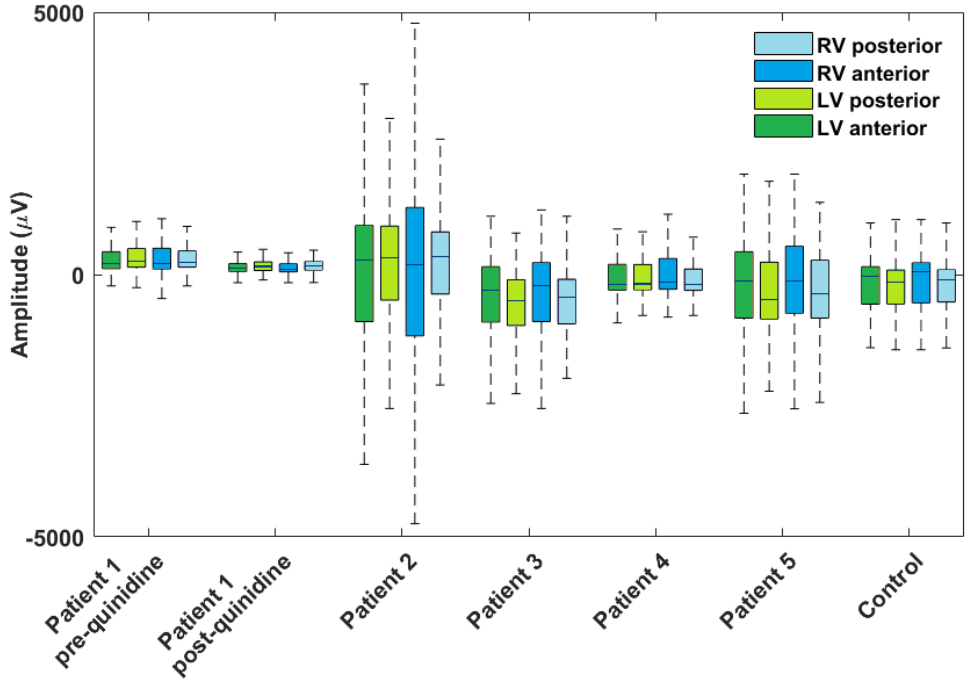

Figure 19 Boxplot demonstrating the distribution of the epicardial amplitude in the left ventricle (LV) anterior, LV posterior, right ventricle (RV) anterior and RV posterior part of the ventricles for each subject.

Amplitude

Figure 19 shows the boxplot from the amplitudes of the T-wave in the RV anterior and posterior part, and the LV anterior and posterior part from the patients with IVF and one control subject. The plot indicates large ranges in amplitude between each subject. The anterior part shows T-waves with higher amplitudes compared to posterior in all subjects except for patient 1. It is remarkable that patient 1 shows exclusively T-waves with a positive amplitude.

For each patient, epicardial amplitude plots with corresponding electrograms can be found in Appendix III. In the anterior view, patient 2, 3, 4 and 5 show negative T-waves in the superior part of the ventricles and change into positive T-waves toward the inferior part, which is similar to the pattern of the control subject. It is remarkable that patient 4 show a similar pattern in the transition from negative to

positive T-waves from respectively superior to inferior in the RV and LV. This can also be seen in the left and right lateral view. In contrast, patient 2, 3 and 5 show T-waves with higher amplitudes in the left lateral ventricle compared to the right lateral ventricle, which is similar to the control subject. Patient 2 exposes a clear region with higher amplitudes in the inferior part of the RV.

In patient 3 and 4, the posterior part of the ventricles contains only T-waves with negative amplitudes, while patient 2 presents positive T-waves in the superior part and negative T-waves inferior. Patient 5 shows negative T-waves in the median part and positive T-waves towards the lateral sides.

Patient 1 shows a different pattern in the distribution of the amplitudes compared to other subjects. In the anterior view, a transition from positive T-waves superior towards negative T-waves inferior can be seen, which is opposite regarding the other subjects. Especially the apex of the LV shows negative T-waves. Next to that, it is remarkable that the superior part of the left and right lateral side contains positive T-waves and change into negative T-waves towards the inferior part. The boxplot demonstrates that the T-wave amplitudes become smaller after quinidine treatment.

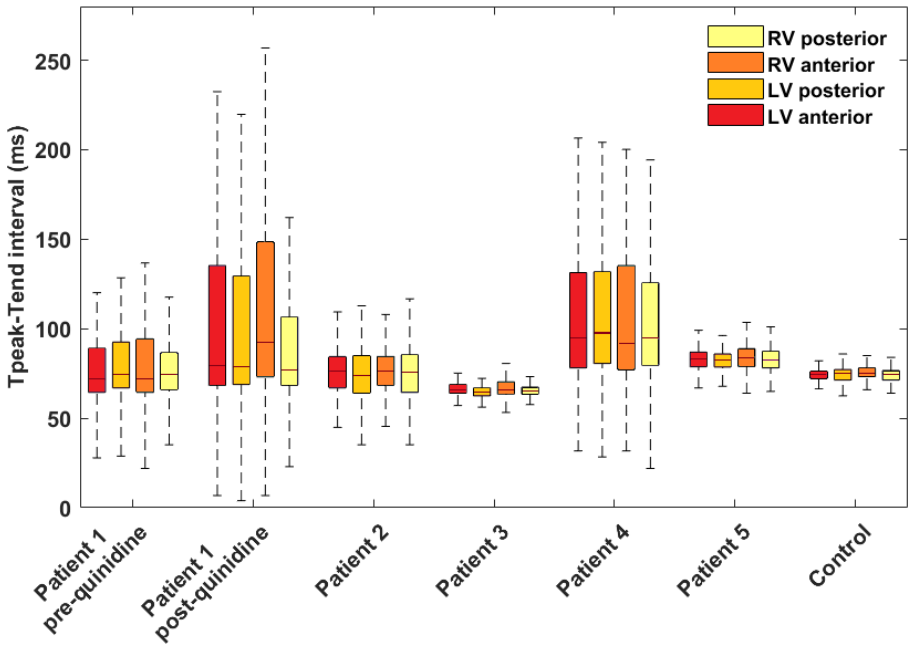

Figure 20 Boxplot demonstrating the distribution of the epicardial Tpeak-Tend interval in the left ventricle (LV) anterior, LV posterior, right ventricle (RV) anterior and RV posterior part of the ventricles for each subject.

Tpeak-Tend interval

Figure 20 shows the boxplot from the Tpeak-Tend intervals of the T-waves in the LV anterior and posterior, and the RV anterior and posterior part from patients with IVF and one control subject. The plot demonstrates a large variety in Tp-e intervals between patient, but intervals show a (nearly) equivalent range in each part of the ventricle in individuals. In patient 1, Tp-e intervals are prolonged after quinidine treatment.

For each patient, epicardial Tp-e interval plots with corresponding electrograms can be found in Appendix III. Areas with prolonged Tp-e intervals are visible in the presence of biphasic T-waves. These regions indicate a transition from positive to negative T-waves. This can be seen clearly in the LV of patient 2 and in both the LV and RV from superior to the apical part in patient 4. In general, patient 1 shows different Tp-e interval areas in both ventricles and electrograms display flat T-waves. Finally, it is remarkable that patients as well as the control subject show different area's in the anterior part. From an anatomical point of view, the fibrous ring can be localized in these areas.

T-wave alternans

Table 3 gives the range of T-wave alternans for all subjects, including values for the median, 25 and 75 percentile and the minimum and maximum value. Patient 5 and the control subject have smaller ranges compared to the other patients, and that the range in T-wave alternans is significantly larger in patient 2.

For each patient, alternans plots with corresponding electrograms can be found in Appendix III.

The plot of patient 1, before quinidine treatment, shows a change in T-wave morphology located in C and D. From the electrogram plot, it becomes clear that the morphology changes in beat 3 and 4. It is remarkable that the T-wave morphology from beat 5 looks similar to the morphology of beat 3. The plot of patient 1, after quinidine treatment, shows minimal changes in T-wave morphology. In the plot of patient 2, an area of changes in T-wave alternans becomes visible in the LV, indicated by the colors red and blue. The electrograms in plot D and E demonstrate a change in T-wave morphology between beat 4, 5 and 6. The plot of patient 3 shows also an area of changing alternans. A difference in morphology is visible between beat 2, 3 and 4. Patient 4 and 5 demonstrate minimal changes in T-wave morphology.

Table 3 Range, median, 25th and 75th percentile of T-wave alternans between two consecutive heartbeats

	25 percentile (µV)	Median (µV)	75 percentile (µV)	Range (µV)
Patient 1 pre-quinidine				
1-2	-57	6	56	-663 – 583
2-3	-46	-0.1	42	-532 – 1094
3-4	-77	11	106	-1375 – 1042
4-5	-84	-9	61	-867 – 877
5-6	-51	-0.6	48	-651 – 622
Patient 1 post-quinidine				
1-2	-26	10	53	-384 – 580
2-3	-74	7	88	-532 – 478
3-4	-72	-10	47	-580 – 515
4-5	-23	13	51	-610 – 572
5-6	-65	14	37	-720 – 582
Patient 2				
1-2	-52	-1	54	-1798 – 916
2-3	-146	-25	123	-1477 – 1499
3-4	-135	10	147	-1514 – 1337
4-5	-140	-22	115	-1682 – 2111
5-6	-111	-34	157	-2055 – 1736
Patient 3				
1-2	-39	22	77	-820 – 643
2-3	-97	-0.1	49	-755 – 577
3-4	-46	-3	59	-468 – 592
4-5	-25	12	42	-608 – 660
5-6	-83	-30	58	-645 – 615
Patient 4				
1-2	-74	-25	25	-777 – 481
2-3	-55	-16	13	-490 – 662
3-4	-55	-16	20	-518 – 611
4-5	-63	-14	69	-726 – 610
5-6	-65	-19	16	-378 – 519
Patient 5				
1-2	-63	0.3	37	-462 – 306
2-3	-38	-11	21	-292 – 398
3-4	-50	7	65	-374 – 424
4-5	-43	5	33	-491 – 273
5-6	-33	15	63	-415 – 347

Control				
1-2	-20	5	33	-303 – 232
2-3	-40	-10	22	-254 – 423
3-4	-27	-0.6	33	-305 – 376
4-5	-53	10	48	-359 – 351
5-6	-28	-10	33	-198 – 404

Late gadolinium enhancement in patients with idiopathic ventricular fibrillation

1 Introduction

In the UMCU and the MUMC, data of nine patients with IVF show LGE on CMR, but the clinical significance has not been defined in these patients. Since LGE in CMR has been found to be prognostic across a variety of cardiac diagnoses and clinical settings, it can be interesting to investigate the clinical significance of LGE in the IVF population. The opportunity to investigate epicardial activation and repolarization using ECGI can give insight in possible abnormalities in this population. It is valuable to investigate similarities between the location of LGE and patterns revealed by ECGI. This might contribute to the verification of LGE in patients with IVF. Therefore, a method for the analysis of LGE. that can be compared to results obtained by ECGI, is proposed in this section.

2 Methods

2.1 Patient population

The study population consists of six patients that were admitted to the hospital due to first episode of VF between 2010 and 2017 who underwent LGE-CMR and received an implantable cardioverter-defibrillator (ICD). All patients were admitted to the department of Cardiology and were clinically evaluated with routine blood test, ECG, echocardiogram, coronary angiogram/ coronary computed tomography to exclude reversible cause of aborted SCA. Four patients are known in the University Medical Center Utrecht and two patients are known in the Maastricht University Medical Center.

2.2 Image acquisition

In four patients, CMR scans were performed between 2010 and 2014 using a 1.5T MRI-scanner designed by Philips Medical Systems, according to the ARVC/D (arrhythmogenic right ventricular cardiomyopathy/dysplasia) protocol from the UMCU. In two patients, CMR scans were performed in 2016 and 2017 using a 1.5T MRI-scanner designed by Siemens Healthcare, according to the ARVC/D (arrhythmogenic right ventricular cardiomyopathy/dysplasia) protocol from the

MUMC. In all cases, patients were scanned approximately 14 days after conversion to sinus rhythm. LGE images were obtained approximately 20 minutes after administration of 0.2 ml Gadovist/kg (1.0 mmol/ml gadubatrol, Gadovist, Bayer HealthCare, Berlin, Germany). A 3D phase-sensitive inversion recovery (PSIR) pulse sequence with navigator-based respiratory gating and ECG-triggering was used. Image characteristics differ between the images of the subjects since scanners from different manufacturers are used, the images are obtained between 2010 and 2017, adjustments in the protocol were made during this time and protocols differ between the medical centers. Slice thickness varied between 6 – 8 mm, number of slices 9 – 15, repetition time 6.07 – 7.08 ms, echo time 1.06 – 3.50 ms, flip angle 25 – 40 $^{\circ}$.

2.3 Image analysis

LGE-CMR images were exported as DICOM-files and analyzed by a PhD student in cardiology/radiology who defined the location of LGE in the images. Next, LGE was quantified by the software tool CARTBox [99]. In general, this software application is used to perform treatment planning for implementation of a CRT device in the heart. CARTBox facilitates the semi-automatically segmentation of the myocardium and LGE area of the left ventricle. Subsequently, a three-dimensional surface mesh of the epi- and endocardial wall of the myocardium is created based on the myocardium segmentation and the segmented area of LGE is projected onto the surface mesh.

3 Results

The results obtained after image analysis with CARTBox are shown in Figure 21. These figures illustrate the diversity in the location of LGE. Furthermore, the extent of transmurality differs between patients.

4 Conclusion

CARTBox is an easy to use software program for analyzing LGE in CMR images. The 3D reconstructions enable comparison of LGE regions with 3D images obtained by ECGI. The possibility to correlate LGE regions with deviating area's measured with ECGI may lead to treatment of these regions with local therapy, such as ablation therapy or the choice for a drug with a specific pathway.

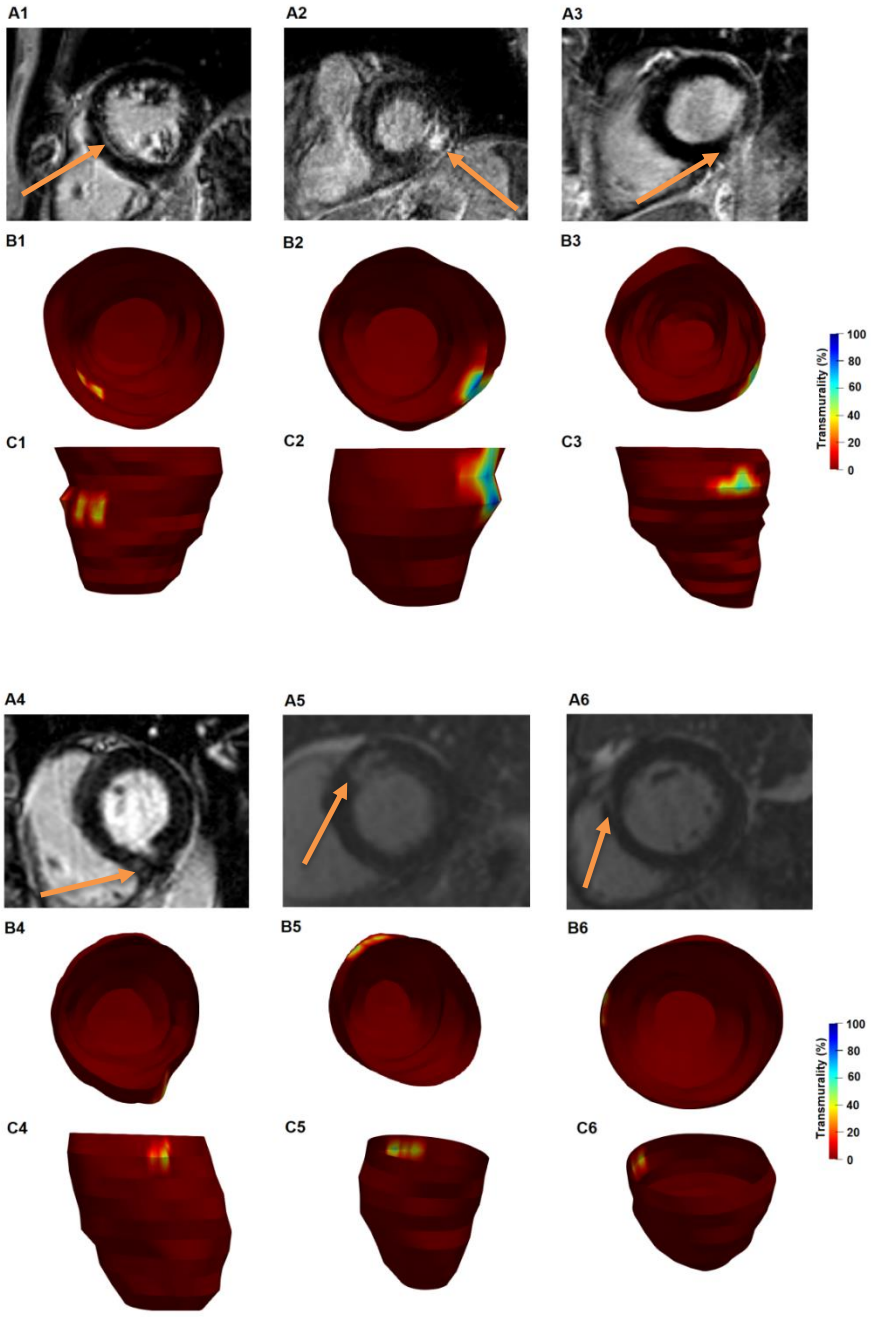

Figure 21 Results after analyzing Late Gadolinium Enhancement in cardiac magnetic resonance images in patients with IVF using CARTBox. The left panel (A1-A3) shows the LGE images. LGE is indicated by the orange arrow. Normally, LGE images can be analyzed over time. The central panel (B1-B3) shows the obtained CARTBox images in a similar view as the LGE images. The right panel (C1-C3) shows the obtained CARTBox images in the posterior view of the left ventricle.

Discussion

A method for calculating various repolarization parameters is developed in this study. This type of analysis is unique at the moment and has not been reported in literature as far as we know. The method shows promising results since the user can check the defined points that are used for calculation of the repolarization parameters. This creates opportunities to discuss results in detail. Next to that, it has been demonstrated that CARTBox is an easy to use software program that provides visualization of LGE in CMR images that can be compared to ECGI results.

1 Repolarization parameters

At this moment, it is not possible to formulate a specific hypothesis regarding the repolarization parameters highlighted in this thesis due to the small study population. Nevertheless, the data shows remarkable results in certain cases. First, patient 1 shows a different pattern in T-wave amplitude compared to the other subjects. Besides, patient 1, 2 and 4 demonstrate an area with a prolonged Tp-e interval in the LV resulting from biphasic T-waves. These biphasic T-waves are also present in the LV of the control subject, but Tp-e intervals are significantly shorter. Furthermore, the T-wave alternans figures reveal a change in T-wave morphology between consecutive heartbeats in patient 1 (before quinidine treatment), 2 and 3. These changes in morphology less evident in patient 1 (during quinidine treatment), 4, 5 and the control subject. However, the figure of patient 1 shows differences in alternans, but this is due to inconsistent T-peak detection as a consequence of the absence of a significant T-peak. These results suggest, together with the information of ICD therapy in these patients (table 2), that Tp-e intervals and T-wave alternans measured with ECGI can provide information about the substrate for the development of VF in IVF and provides a foundation for further exploration of the repolarization characteristic in a larger study population and in control subjects.

2 Algorithm

The recorded body surface potentials were filtered before the algorithm for T-peak detection was applied. Choices for filtering were based on signals that

contained noise already and the noise-free signals were unknown. In general, it is difficult to objectively evaluate filter performance based on modifications of the ST-segment. In this thesis, choices for signal filtering are based on amplitude spectra, visual improvement and results from filtering techniques demonstrated in literature [84].

The algorithm includes a method for comparison of electrograms and corresponding detected T-peaks at the vertices of each triangle on the surface mesh. False detected peaks can be adapted manually by the user as a result of this method. A disadvantage of manual adjustments is the consequence of differences in results of repolarization parameters between different users. To overcome this problem, the tool for visualization of the electrograms on the mesh surface is introduced. This enables users to look into detail in determined parameters.

2.1 Validation

The validation of the algorithm shows sensitivity of 75.5% and 93.5% regarding observer 1 and 2 respectively for the determination of the primary T-peak. The lower sensitivity value regarding observer 1 is a result of inaccurate annotations of peaks. Next to that, the low sensitivity for determination of the end of the T-wave is remarkable. Literature and discussions with physicians clarified that there is no consensus about the determination of the T-wave end, especially in ECGI [77], [92], [94]. This disagreement is also elucidated by the method for validation, since observers agree in 26% of the cases about the T-wave end.

3 ECGI

Several discussion points came up during this research regarding the use of ECGI.

First, it appeared that the reconstructions of unipolar electrograms on the right lateral side of the ventricles are corrupted in some cases (see figure 32, 34, 35 and 41). This can be due to insufficient recording of body surface potentials on the right side of the body. Body surface measurements that include bad signals are removed before reconstructions are calculated. It is possible that recordings at the right side are removed because of insufficient recording and results eventually in poor reconstructions at this side of the epicardium. Another possibility includes the increased distance between the body surface measurement electrodes and the epicardial surface at the right side of the body compared to the left and anterior side.

These poor reconstructions lead also to inaccurate determination of the baseline, what can result in inappropriate T-peak and T-end detection by the algorithm. Next to that it can result in inappropriate interpretation of repolarization patterns, since poor reconstruction can lead to signals that seem to be biphasic but are monophasic originally. Especially the determination of the Tpeak-Tend interval will suffer from this.

In this work, the presence of the U-wave is not considered. When a U-wave is present, this can affect the calculation of the level of the baseline. For example, a positive U-wave can lead to higher level baseline.

The algorithm includes a part for a check of neighbouring signals on the surface mesh. It appeared that signals differ significantly at the vertices of one triangle in some cases. An example is given in Appendix I in Figure 23. In general, signals with low correlation have low amplitudes or the reconstructions are poor.

The plots of the reconstructed epicardial surfaces for each patient in depicted in the section results and Appendix III demonstrate that the shape of the ventricles differ between subjects. In ECGI, the epicardium is manually segmented from CT-scans. This can result in different epicardial surfaces between users. The question arises what the influence of the reconstructed epicardial surface will be on the reconstruction of the unipolar electrograms. It is recommended to investigate this by segmenting the epicardium by two observers and apply the reconstructions on both meshes. Furthermore, it would be valuable to implement a tool for automatic segmentation of the epicardium to overcome this problem.

Another point for discussion in ECGI includes the assumption that both heart and torso are non-moving. The static torso-hear geometry is usually based on a CT-scan during cardiac diastole and breath hold, to capture both heart and torso in a quiescent state. However, during the recording of the body surface potentials that are used for inverse reconstruction, both torso and heart are changing in geometry. This false assumption can lead to inappropriate reconstructions of the electrograms. The influence of movement should be investigated.

4 Late Gadolinium Enhancement in idiopathic ventricular fibrillation

CARTBox enables the user to visualize LGE easily in the left ventricle, but it is not applicable in the right ventricle. This limited analysis of LGE in one patient with IVF in this study.

The clinical significance of LGE in IVF patients is not yet established and LGE regions are reported as suspicious by radiologists. The reconstruction of the 3D plot of the left ventricle enables clinicians to compare LGE regions with results from ECGI. It is possible that abnormalities in ECGI can clarify the presence of LGE in these patients. It is recommended to discuss results with cardiologists as well as radiologists. However, for comparison of CARTBox images with ECGI images, it needs to be considered that LGE CMR images contain approximately 12 slices, while the reconstruction of the ventricles in ECGI includes more slices from the CT-scan what results in a higher resolution.

The MUMC provided LGE CMR data from five IVF patients, but the data of three patients could not be analyzed due to artifacts in images and incorrect datasets.

5 Future work

The value of ECGI in idiopathic ventricular fibrillation will be investigated in the VIGILANCE project. It is known that the IVF population includes a heterogeneous group and the aim of the project is to differentiate between substrates that can lead to VF and to improve risk stratification in this population and their relatives.

The clinical significance of repolarization parameters in ECGI is unknown at the moment. For example, it is unknown whether the Tpeak-Tend interval contains similar information as on the 12-lead ECG. It is recommended to investigate these repolarization patterns in diseases that are more established, for example in LQTS. Furthermore, it can be investigated whether patients with a prolonged Tpeak-Tend interval on the ECG present also a prolonged interval in ECGI.

In literature, different opinions about the determination of the location of points in the T-wave are elucidated [22], [56], [57], [62], [77], [94], [98]. For further research with ECGI, it is recommended to achieve a nationwide consensus about these points. This can create opportunities for collaboration between different research groups but also the ability to compare results in different diseases. In the Netherlands, both CT and MRI are used for the reconstruction of the heart-torso geometry in different research groups. It is recommended to compare these methods and to investigate the influence on results.

When abnormalities in repolarization are found in patients with IVF using ECGI, it is recommended to verify results by intracardiac mapping. This will also

contribute to validation of ECGI. However, at this moment, no specific hypothesis can be formulated about the mentioned repolarization parameters and their correlation with the development of VF in IVF. First, these parameters should be investigated in a control patient.

Despite the challenges, ECGI may be a promising tool to complement conventional electrophysiological studies. For example, in patients suffering from arrhythmias, substrates may be localized using ECGI prior to the ablation procedure. This can lead to a reduction in the duration of the procedure and can contribute to a decrease in exposure to radiation. ECGI can also play a role in the understanding of the development of heart diseases and the contribution to the electrical behavior of the myocardium. This may lead to an improvement in informing patients about their disease progression and future perspectives. Furthermore, the technique can play a role in optimization of pacing therapy. Knowledge of anatomy, location of scar tissue and information about activation and recovery behavior can serve as a predictor for optimal lead placement.

Appendix I

Methods for de-noising body surface potentials

Four different filtering techniques that are often proposed in literature are compared: Butterworth zero-phase filtering, moving median filtering, morphological filtering and wavelet-based filtering. A brief introduction to each method is given in this section.

Butterworth zero-phase band-pass filtering

First, a Butterworth band-pass filter with a total order of four and a band-pass frequency between 0.5 Hz and 40 Hz is applied, using the MATLAB function butter. Zero-phase filtering is applied, which means that the input data is filtered in forward and reverse direction, resulting in zero phase distortion. Actually, the transfer function of the filter had an order of two, but the zero-phase filtering process results in an order of four.

Moving median filtering

The aim of this method is to estimate baseline wander by two moving median filters and subtracting the estimation from the original signal. The moving median is based on the same principle as the moving average, where data points are analyzed by creating a series of averages of different subsets of the full data set. However, in the moving median approach, the median within a moving window is used instead of the mean. From a statistical point of view, the moving median approach suits better for ECG signals compared to a moving mean approach, because of the possibility of rapid movements in the signal.

The removal technique started with a window length of 200 ms, since the T-wave should not exceed this time interval. Since windows of this short duration can deliver an estimation that is a mixture of true ECG signal and baseline, a second moving median with a window of a longer length was applied after the first estimation. For this, a window length of 600 ms was chosen. By doing so, the inclusion of both the depolarization and repolarization of the ventricles is ensured.

Morphological filtering

Mathematical morphology (MM), which is strictly based on mathematical disciplines, provides an effective non-linear signal processing method and can keep the shape information of the signal information good. Structuring elements are the basic concept of MM, which has a certain form (such as point, line, circle etc.). By using a structuring element to operate on a signal, the information of a signal (shape, size etc.) can be extracted. Different forms of structuring elements result in different outcomes. There are two basic morphological operators: erosion and dilation. Opening and closing are derived operators in terms of erosion and dilation. Opening and closing operators can be interpreted as sliding structuring elements along the signal from beneath and above respectively and the result is the highest and the lowest point reached by any part of the structuring element. Opening operation is used to remove peaks from the signal; closing is used to remove the valleys. [100], [101]

In this thesis, the length of the opening operator is chosen as 200 ms, because this value is greater than the width of the characteristic waves of the ECG signal (P, Q, R, S and T-wave individually). The length of the closing operator should be longer than the length of the opening operator and is typically selected to be 1.5 times the length of the opening operator. In this case, the closing operator is chosen as 300 ms.

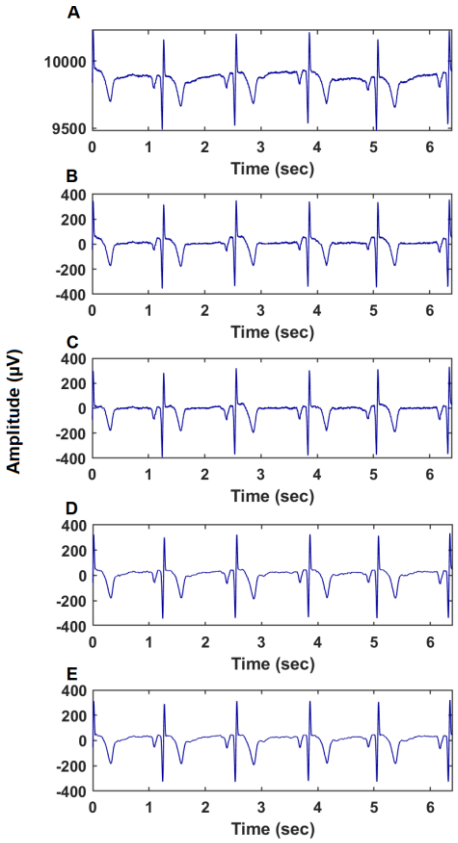

Figure 22 Example of a body surface potential measurement by different filtering techniques: (A) unfiltered signal (B) signal after application of morphological filtering (C) signal after application of a moving median filtering (D) signal after Butterworth band-pass filtering (E) signal after wavelet filtering

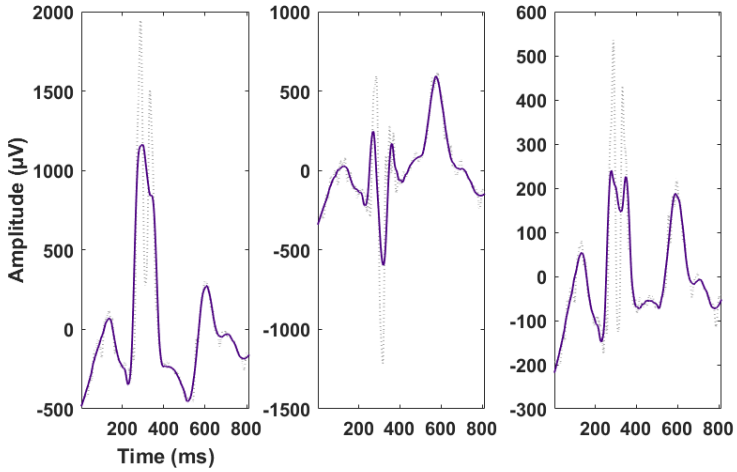

Figure 23 Example of three signals located on the vertices of one triangle in the epicardial mesh.

Appendix II

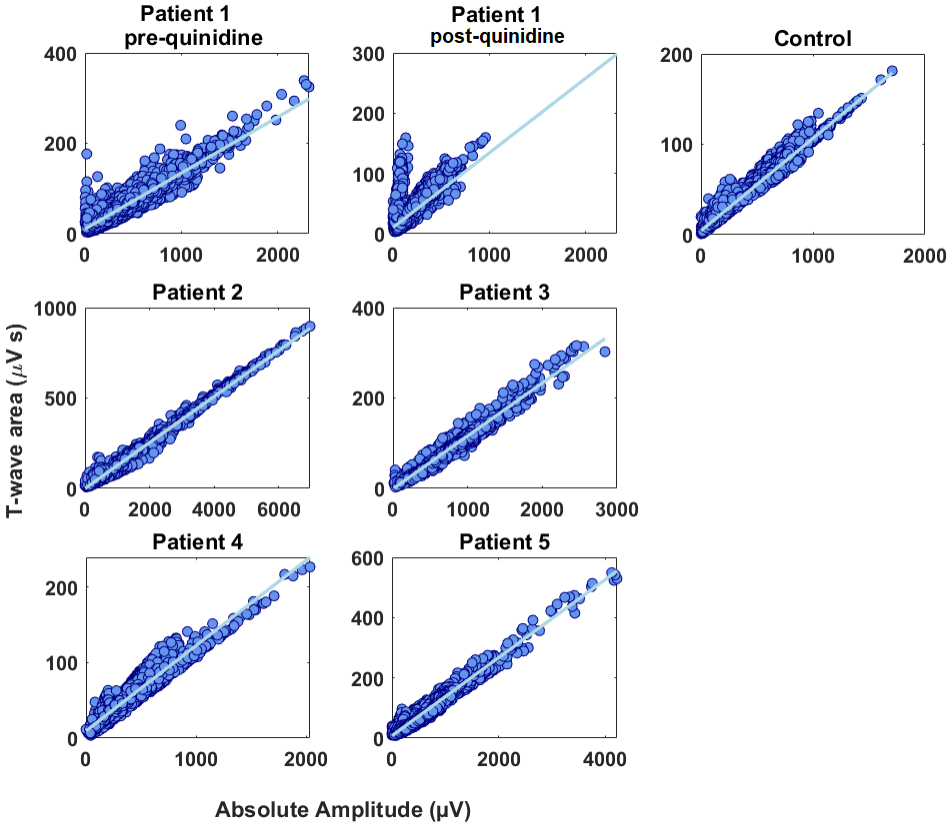

Figure 24 Linear correlation between the absolute amplitude and the area of the epicardial T-waves reconstructed with ECGI for each subject.

Appendix III

Patient 1 pre-quinidine – Amplitude

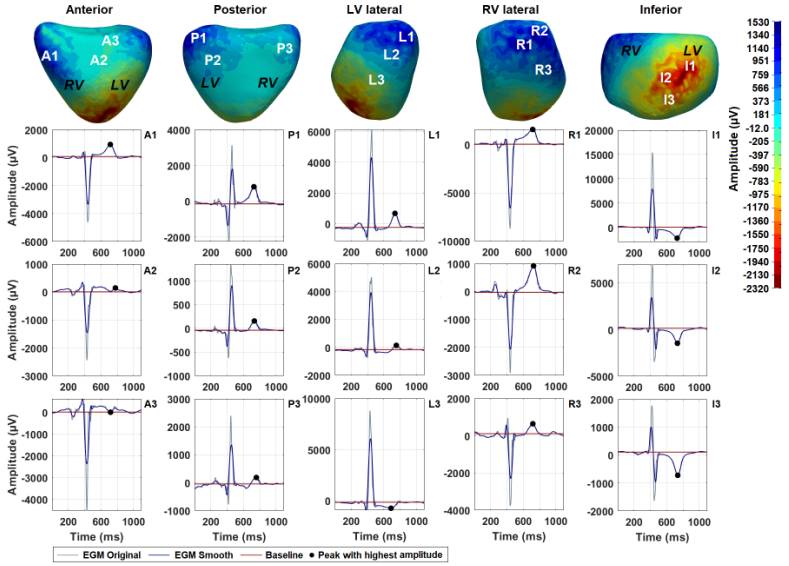

Figure 25 Epicardial amplitude maps of patient 1 pre-quinidine treatment, reconstructed with ECGI. The left panel shows the 3D epicardial surface of the left ventricle (LV) and right ventricle (RV) from the anterior, posterior, left and right lateral and inferior view. The right panel shows the electrograms that correspond to the marked areas in the left panel. Example; electrogram A1 is localized in the "A1" marked area in the anterior view.

Patient 1 pre-quinidine – Tpeak-Tend interval

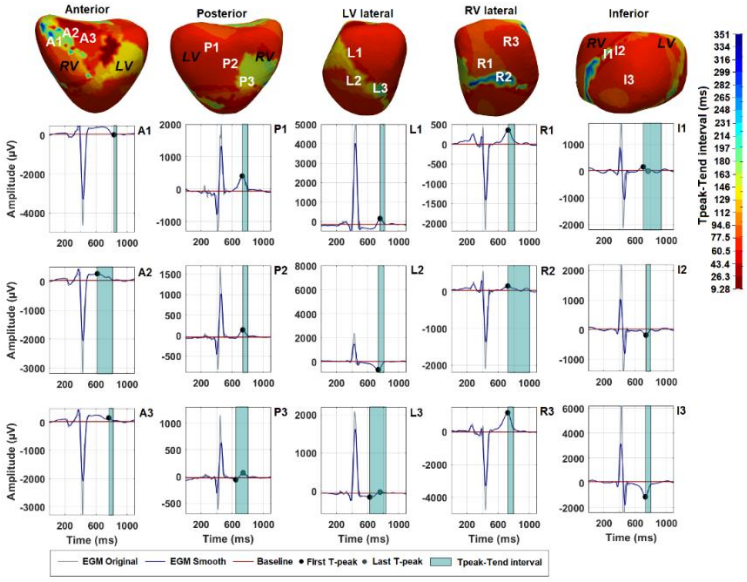

Figure 26 Epicardial Tpeak-Tend interval maps of patient 1 pre-quinidine treatment, reconstructed with ECGI. The left panel shows the 3D epicardial surface of the left ventricle (LV) and right ventricle (RV) from the anterior, posterior, left and right lateral and inferior view. The right panel shows the electrograms that correspond to the marked areas in the left panel. Example; electrogram A1 is localized in the "A1" marked area in the anterior view.

Patient 1 pre-quinidine – Alternans

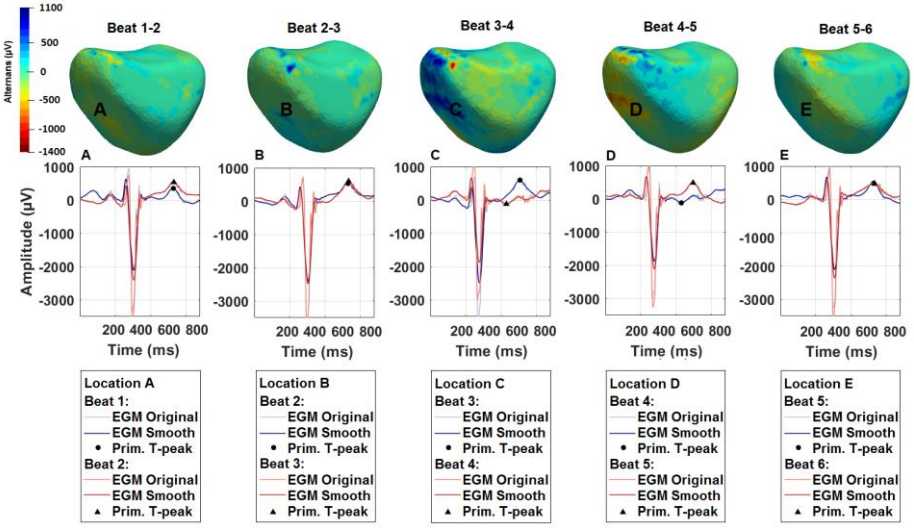

Figure 27 Epicardial T-wave alternans maps of patient 1 pre-quinidine treatment, reconstructed with ECGI. The difference in T-peak amplitude is calculated for six consecutive beats. The letters A - E indicate the location of the epicardial electrogram. This location is equal for each heartbeat. The horizontal, central plane shows the electrograms for each set of beats.

Patient 1 post-quinidine – Amplitude

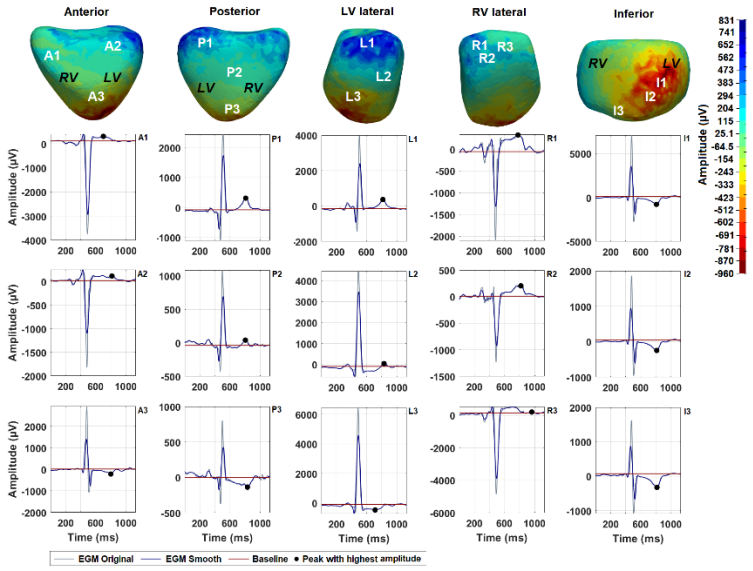

Figure 28 Epicardial amplitude maps of patient 1 post-quinidine treatment, reconstructed with ECGI. The left panel shows the 3D epicardial surface of the left ventricle (LV) and right ventricle (RV) from the anterior, posterior, left and right lateral and inferior view. The right panel shows the electrograms that correspond to the marked areas in the left panel. Example; electrogram A1 is localized in the "A1" marked area in the anterior view.

Patient 1 post-quinidine – Tpeak-Tend interval

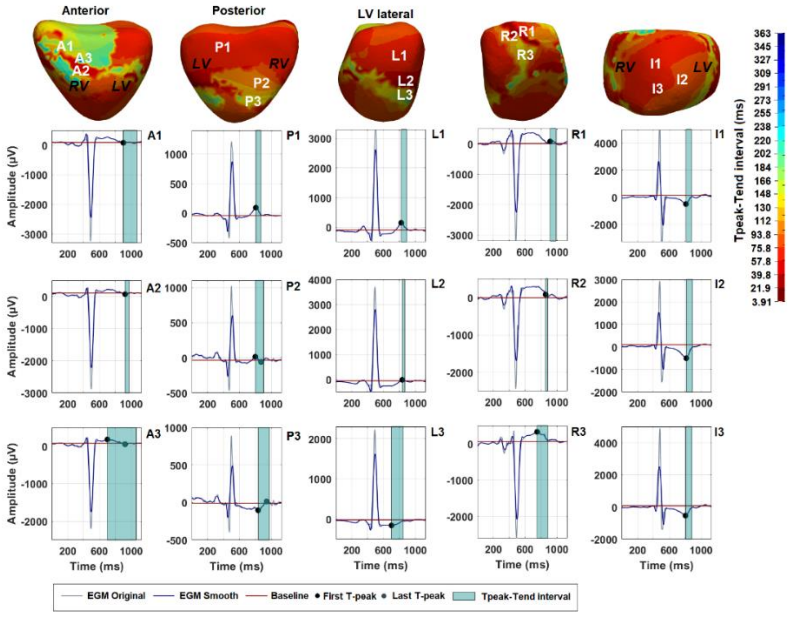

Figure 29 Epicardial Tpeak-Tend interval maps of patient 1 post-quinidine treatment, reconstructed with ECGI. The left panel shows the 3D epicardial surface of the left ventricle (LV) and right ventricle (RV) from the anterior, posterior, left and right lateral and inferior view. The right panel shows the electrograms that correspond to the marked areas in the left panel. Example; electrogram A1 is localized in the "A1" marked area in the anterior view.

Patient 1 post-quinidine – Alternans

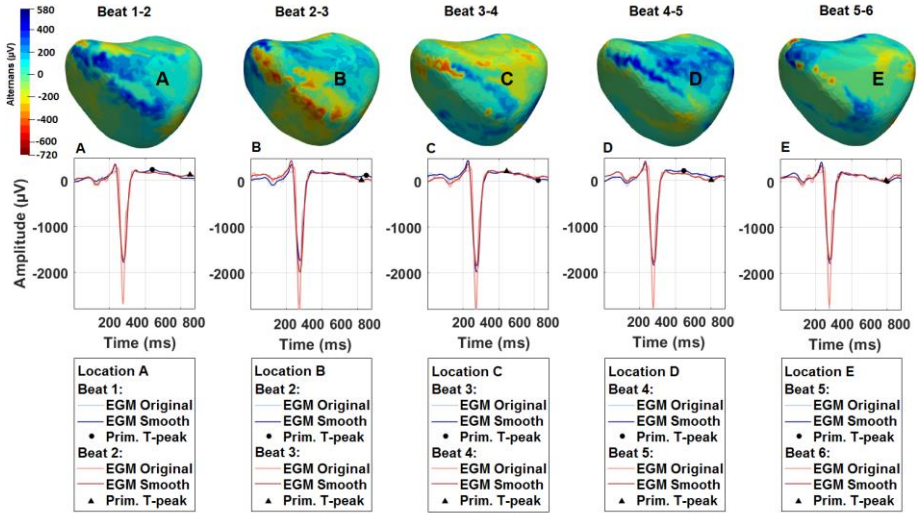

Figure 30 Epicardial T-wave alternans maps of patient 1 post-quinidine treatment, reconstructed with ECGI. The difference in T-peak amplitude is calculated for six consecutive beats. The letters A - E indicate the location of the epicardial electrogram. This location is equal for each heartbeat. The horizontal, central plane shows the electrograms for each set of beats.

Patient 2 Amplitude

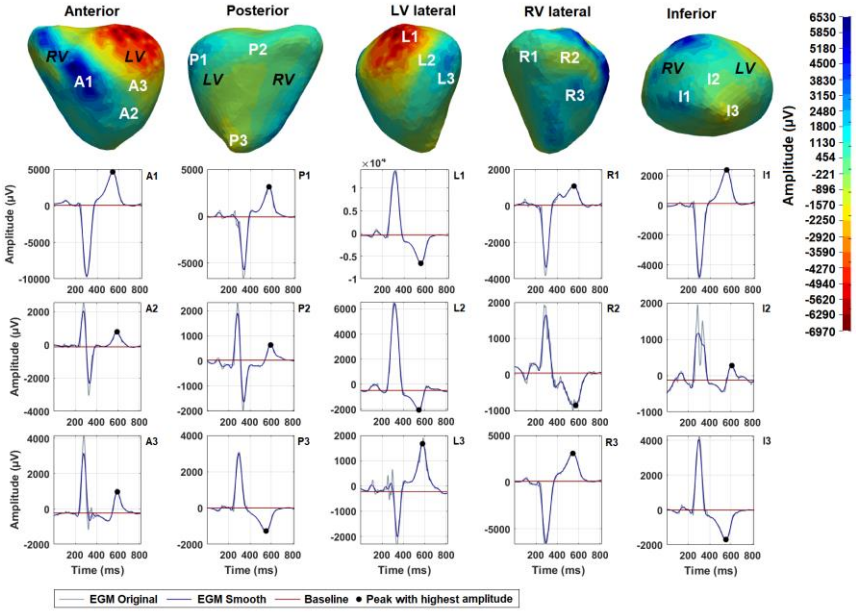

Figure 31 Epicardial amplitude maps of patient 2, reconstructed with ECGI. The left panel shows the 3D epicardial surface of the left ventricle (LV) and right ventricle (RV) from the anterior, posterior, left and right lateral and inferior view. The right panel shows the electrograms that correspond to the marked areas in the left panel. Example; electrogram A1 is localized in the "A1" marked area in the anterior view.

Patient 2 Tpeak-Tend interval

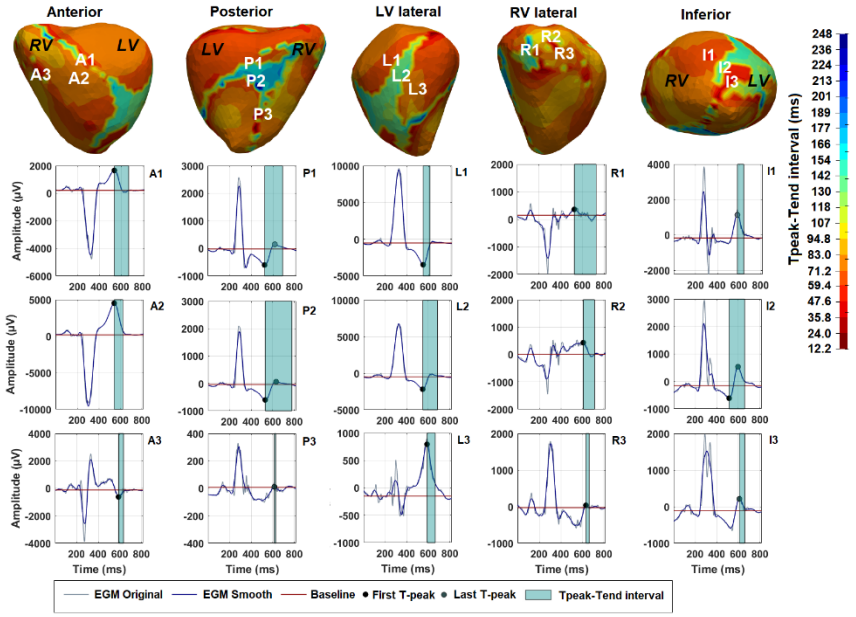

Figure 32 Epicardial Tpeak-Tend interval maps of patient 2, reconstructed with ECGI. The left panel shows the 3D epicardial surface of the left ventricle (LV) and right ventricle (RV) from the anterior, posterior, left and right lateral and inferior view. The right panel shows the electrograms that correspond to the marked areas in the left panel. Example; electrogram A1 is localized in the "A1" marked area in the anterior view.

Patient 2 Alternans

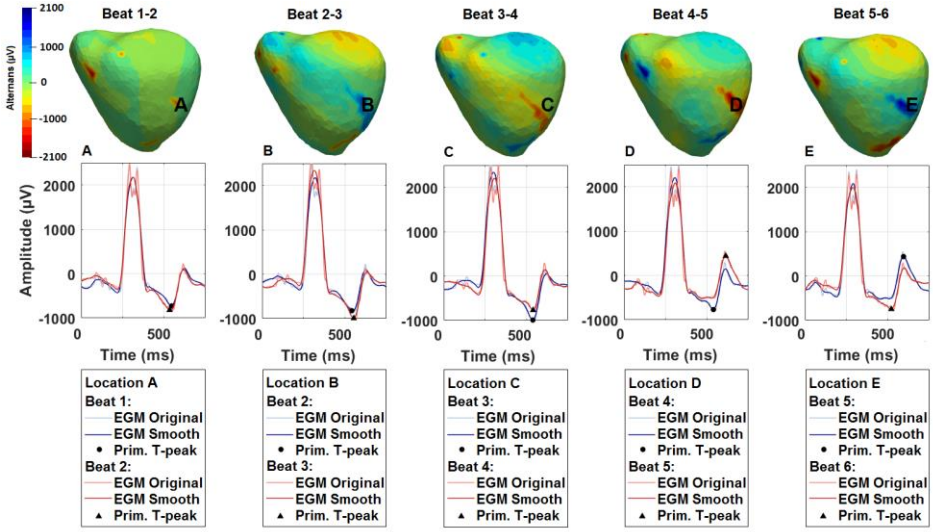

Figure 33 Epicardial T-wave alternans maps of patient 2, reconstructed with ECGI. The difference in T-peak amplitude is calculated for six consecutive beats. The letters A - E indicate the location of the epicardial electrogram. This location is equal for each heartbeat. The horizontal, central plane shows the electrograms for each set of beats.

Patient 3 Amplitude

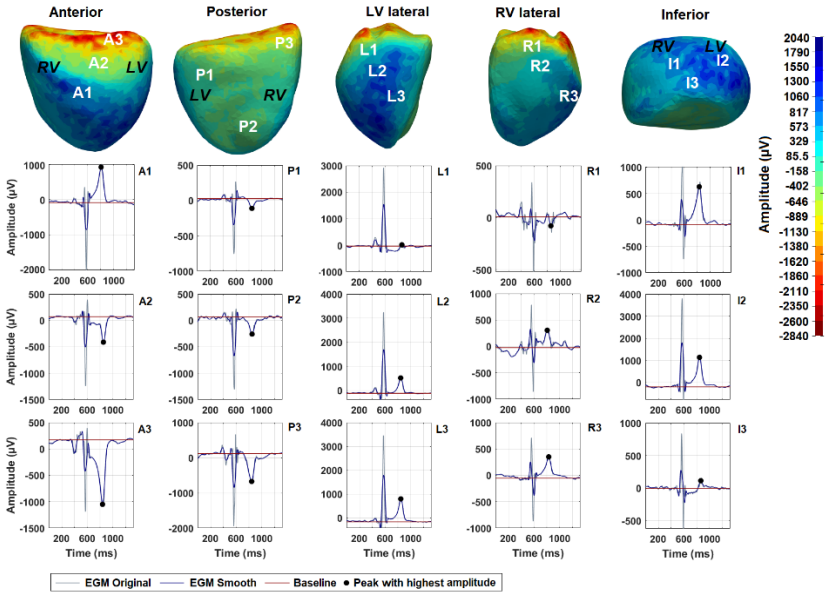

Figure 34 Epicardial amplitude maps of patient 3, reconstructed with ECGI. The left panel shows the 3D epicardial surface of the left ventricle (LV) and right ventricle (RV) from the anterior, posterior, left and right lateral and inferior view. The right panel shows the electrograms that correspond to the marked areas in the left panel. Example; electrogram A1 is localized in the "A1" marked area in the anterior view.

Patient 3 Tpeak-Tend interval

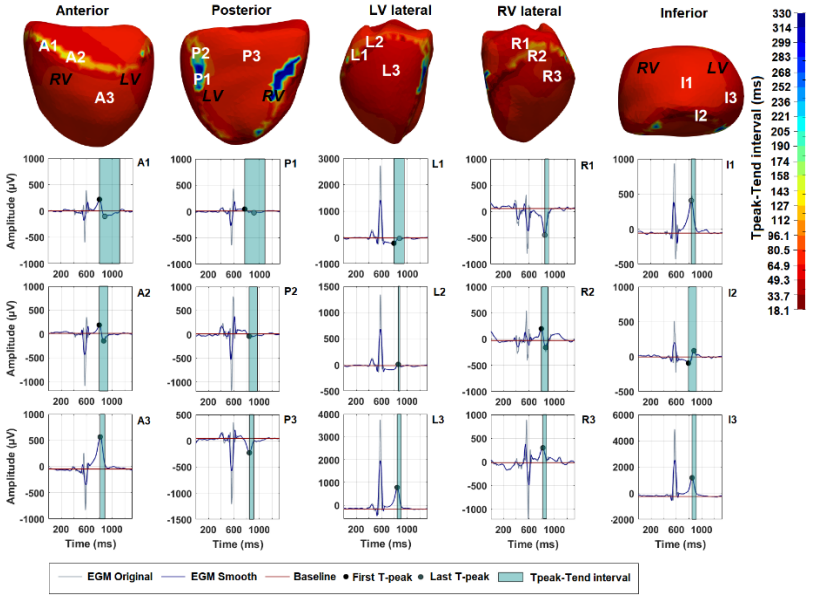

Figure 35 Epicardial Tpeak-Tend interval maps of patient 3, reconstructed with ECGI. The left panel shows the 3D epicardial surface of the left ventricle (LV) and right ventricle (RV) from the anterior, posterior, left and right lateral and inferior view. The right panel shows the electrograms that correspond to the marked areas in the left panel. Example; electrogram A1 is localized in the "A1" marked area in the anterior view.

Patient 3 Alternans

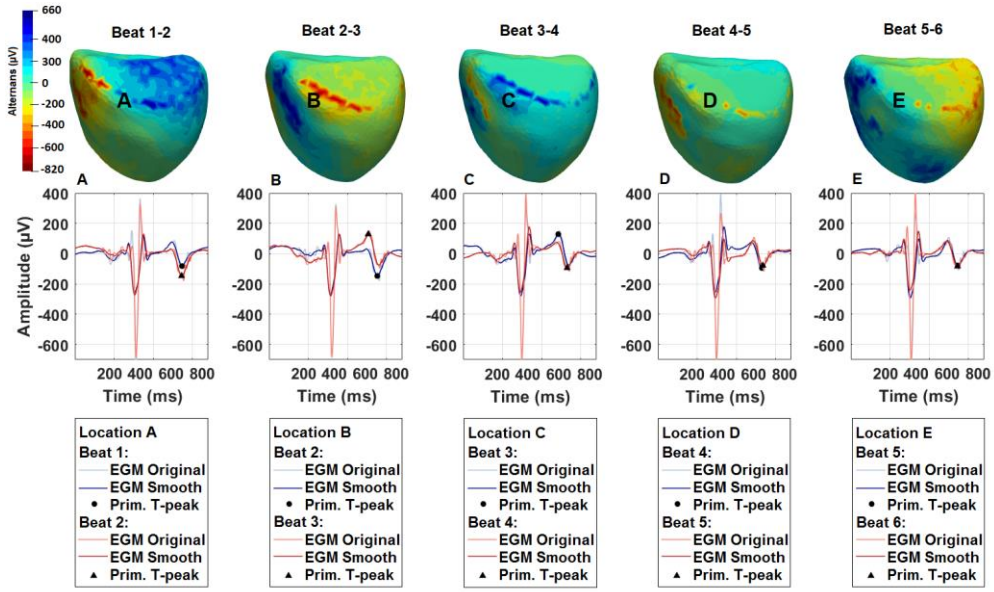

Figure 36 Epicardial T-wave alternans maps of patient 3, reconstructed with ECGI. The difference in T-peak amplitude is calculated for six consecutive beats. The letters A - E indicate the location of the epicardial electrogram. This location is equal for each heartbeat. The horizontal, central plane shows the electrograms for each set of beats.

Patient 4 Amplitude

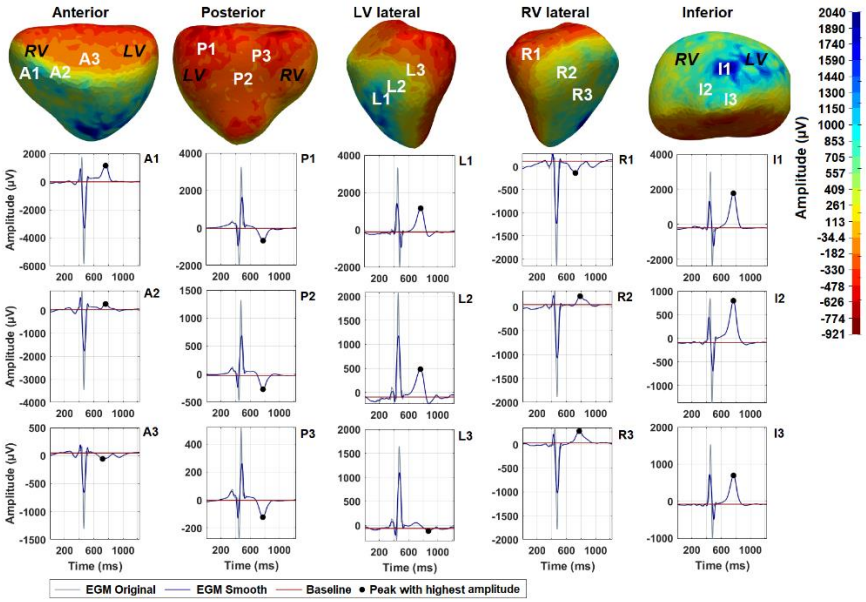

Figure 37 Epicardial amplitude maps of patient 4, reconstructed with ECGI. The left panel shows the 3D epicardial surface of the left ventricle (LV) and right ventricle (RV) from the anterior, posterior, left and right lateral and inferior view. The right panel shows the electrograms that correspond to the marked areas in the left panel. Example; electrogram A1 is localized in the "A1" marked area in the anterior view.

Patient 4 Tpeak-Tend interval

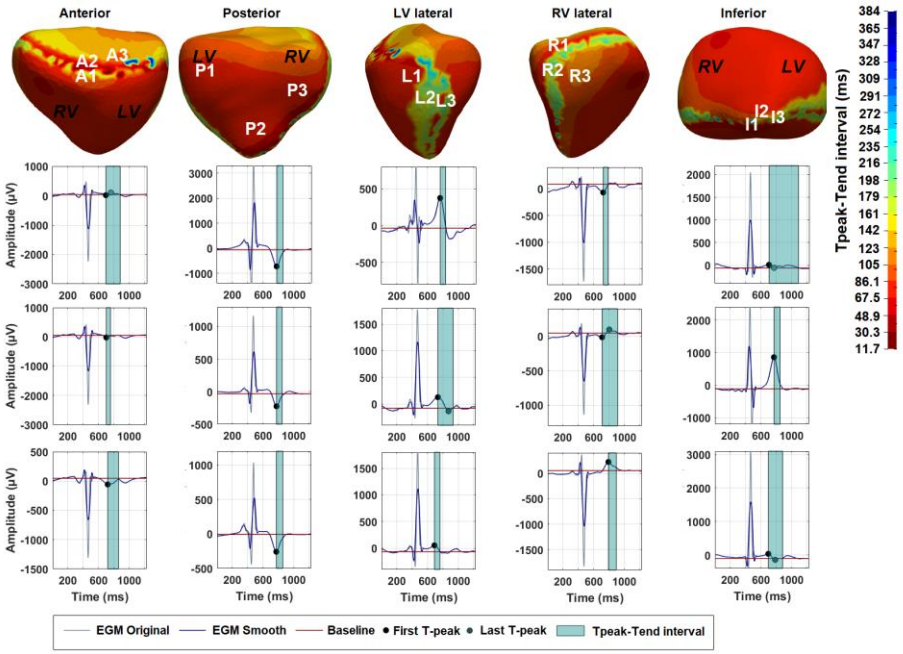

Figure 38 Epicardial Tpeak-Tend interval maps of patient 4, reconstructed with ECGI. The left panel shows the 3D epicardial surface of the left ventricle (LV) and right ventricle (RV) from the anterior, posterior, left and right lateral and inferior view. The right panel shows the electrograms that correspond to the marked areas in the left panel. Example; electrogram A1 is localized in the "A1" marked area in the anterior view.

Patient 4 Alternans

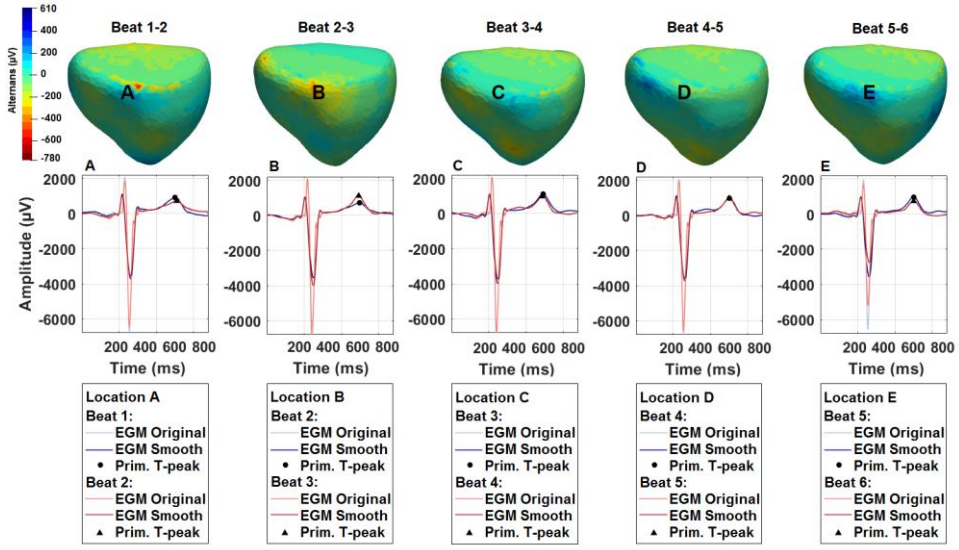

Figure 39 Epicardial T-wave alternans maps of patient 4, reconstructed with ECGI. The difference in T-peak amplitude is calculated for six consecutive beats. The letters A - E indicate the location of the epicardial electrogram. This location is equal for each heartbeat. The horizontal, central plane shows the electrograms for each set of beats.

Patient 5 Amplitude

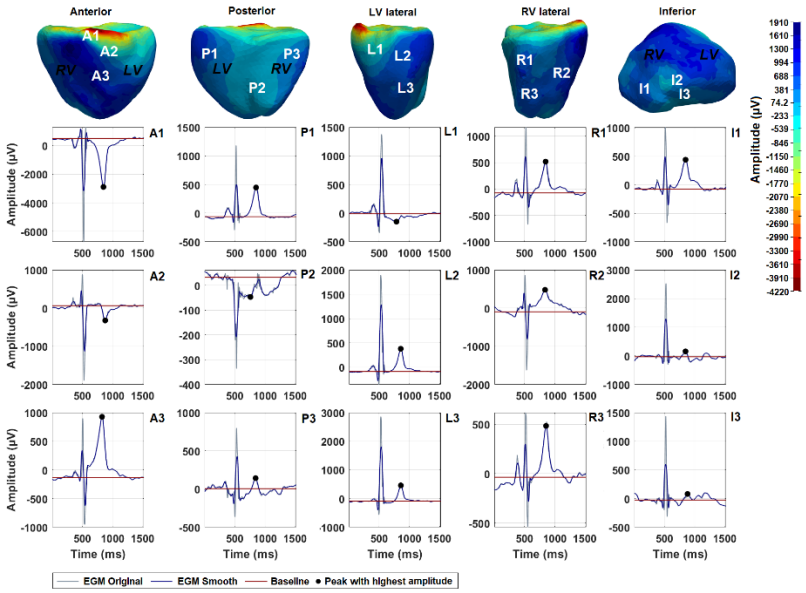

Figure 40 Epicardial amplitude maps of patient 5, reconstructed with ECGI. The left panel shows the 3D epicardial surface of the left ventricle (LV) and right ventricle (RV) from the anterior, posterior, left and right lateral and inferior view. The right panel shows the electrograms that correspond to the marked areas in the left panel. Example; electrogram A1 is localized in the "A1" marked area in the anterior view.

Patient 5 Tpeak-Tend interval

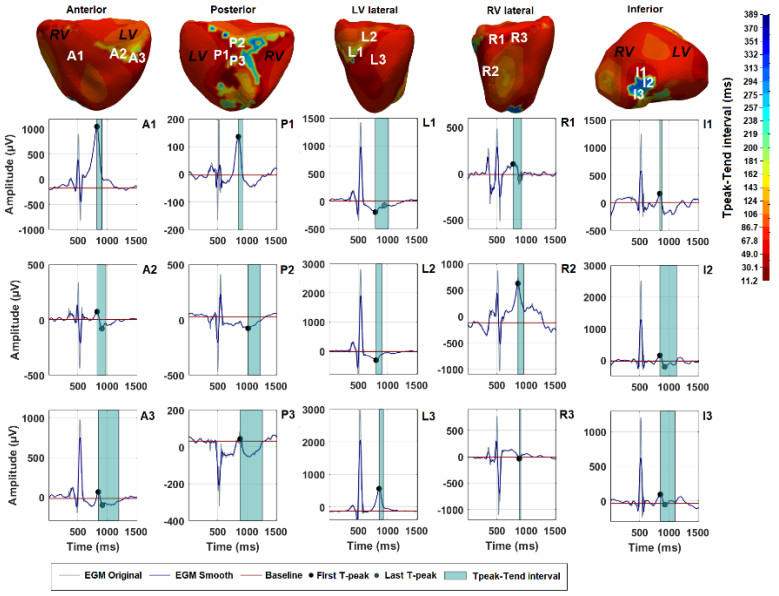

Figure 41 Epicardial Tpeak-Tend interval maps of patient 5, reconstructed with ECGI. The left panel shows the 3D epicardial surface of the left ventricle (LV) and right ventricle (RV) from the anterior, posterior, left and right lateral and inferior view. The right panel shows the electrograms that correspond to the marked areas in the left panel. Example; electrogram A1 is localized in the "A1" marked area in the anterior view.

Patient 5 Alternans

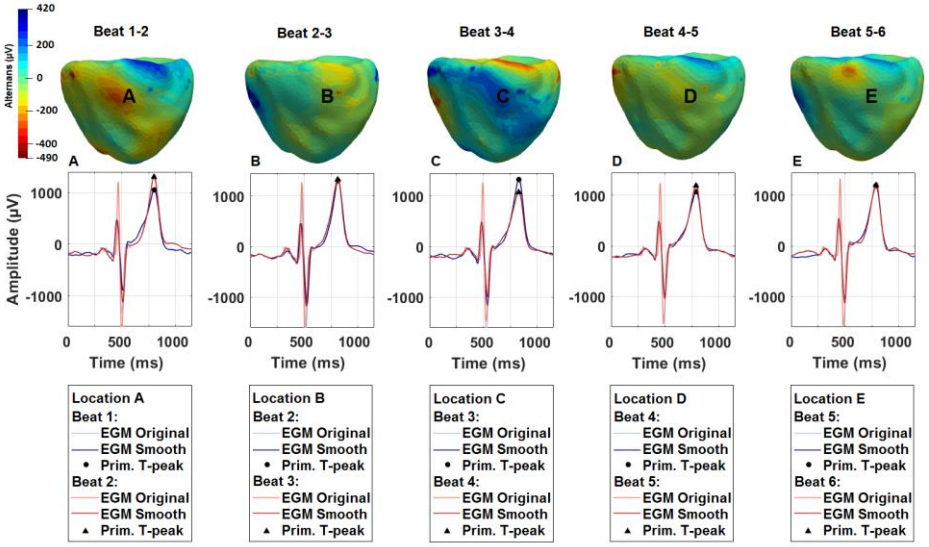

Figure 42 Epicardial T-wave alternans maps of patient 5, reconstructed with ECGI. The difference in T-peak amplitude is calculated for six consecutive beats. The letters A - E indicate the location of the epicardial electrogram. This location is equal for each heartbeat. The horizontal, central plane shows the electrograms for each set of beats.

References

[1] S. M. J. M. Straus, G. S. Bleumink, J. P. Dieleman, J. Lei Van Der, B. H. C. Stricker, and M. C. J. M. Sturkenboom, "The incidence of sudden cardiac death in the general population," *J. Clin. Epidemiol.*, vol. 57, no. 1, pp. 98–102, 2004.

[2] S. G. Priori *et al.*, "HRS/EHRA/APHRS Expert Consensus Statement on the Diagnosis and Management of Patients with Inherited Primary Arrhythmia Syndromes: Document endorsed by HRS, EHRA, and APHRS in May 2013 and by ACCF, AHA, PACES, and AEPC in June 2013.," *Hear. Rhythm*, vol. 10, no. 12, pp. 1932–1963, Dec. 2013.

[3] L. J. Blom, P.G.A. Volders, A.A. Wilde, and R.J. Hassink, "Life-long tailoring of diagnosis and management of patients with idiopathic ventricular fibrillation-future perspectives in research," *Netherlands Hear. J.*, 2018.

[4] M. Visser *et al.*, "Long-Term Outcome of Patients Initially Diagnosed with Idiopathic Ventricular Fibrillation," *Circ. Arrhythmia Electrophysiol.*, vol. 9, no. 10, p. e004258, 2016.

[5] Y. Rudy, "Noninvasive ECG imaging (ECGI): Mapping the arrhythmic substrate of the human heart," *Int. J. Cardiol.*, vol. 237, pp. 13–14, 2017.

[6] Y. Rudy, "Noninvasive electrocardiographic imaging of arrhythmogenic substrates in humans," *Circ. Res.*, vol. 112, no. 5, pp. 863–874, 2013.

[7] J. E. Burnes, R. N. Ghanem, A. L. Waldo, and Y. Rudy, "Imaging dispersion of myocardial repolarization, I: Comparison of body-surface and epicardial measures," *Circulation*, vol. 104, no. 11, pp. 1299–1305, 2001.

[8] M. Sugao *et al.*, "Repolarization dynamics in patients with idiopathic ventricular fibrillation: Pharmacological therapy with bepridil and disopyramide," *J. Cardiovasc. Pharmacol.*, vol. 45, no. 6, pp. 545–549, 2005.

[9] K. M. Leong *et al.*, "Repolarization abnormalities unmasked with exercise in sudden cardiac death survivors with structurally normal hearts," *J. Cardiovasc. Electrophysiol.*, vol. 29, no. 1, pp. 115–126, 2018.

[10] M. J. M. Cluitmans *et al.*, "In Vivo Validation of Electrocardiographic Imaging," *JACC Clin. Electrophysiol.*, vol. 3, no. 3, pp. 232–242, Mar. 2017.

[11] P. Brugada and J. Brugada, "Right bundle branch block, persistent ST

segment elevation and sudden cardiac death: A distinct clinical and electrocardiographic syndrome. A multicenter report," *J. Am. Coll. Cardiol.*, 1992.

[12] S. G. Priori *et al.*, "Clinical and molecular characterization of patients with catecholaminergic polymorphic ventricular tachycardia," *Circulation*, 2002.

[13] A. Medeiros-Domingo *et al.*, "Gain-of-function mutation S422L in the KCNJ8-encoded cardiac KATPchannel Kir6.1 as a pathogenic substrate for J-wave syndromes," *Hear. Rhythm*, 2010.

[14] I. Gussak *et al.*, "Idiopathic Short QT Interval: A New Clinical Syndrome?," *Cardiology*, vol. 94, no. 2, pp. 99–102, 2000.

[15] M. J. Ackerman *et al.*, "HRS/EHRA expert consensus statement on the state of genetic testing for the channelopathies and cardiomyopathies: This document was developed as a partnership between the Heart Rhythm Society (HRS) and the European Heart Rhythm Association (EHRA)," *Hear. Rhythm*, vol. 8, no. 8, pp. 1308–1339, 2011.

[16] M. Alders *et al.*, "Haplotype-Sharing Analysis Implicates Chromosome 7q36 Harboring DPP6 in Familial Idiopathic Ventricular Fibrillation," *Am. J. Hum. Genet.*, vol. 84, no. 4, pp. 468–476, 2009.

[17] R. F. Marsman *et al.*, "A mutation in CALM1 encoding calmodulin in familial idiopathic ventricular fibrillation in childhood and adolescence," *J. Am. Coll. Cardiol.*, vol. 63, no. 3, pp. 259–266, 2014.

[18] J. Han and G. K. Moe, "Nonuniform Recovery of Excitability in Ventricular Muscle.," *Circ. Res.*, vol. 14, no. January, pp. 44–60, 1964.

[19] D. M. Mirvis, "Spatial variation of QT intervals in normal persons and patients with acute myocardial infarction," *J. Am. Coll. Cardiol.*, vol. 5, no. 3, pp. 625–631, 1985.

[20] C. Patel *et al.*, "Is there a significant transmural gradient in repolarization rime in the intact heart? Cellular basis of the Twave: a century of controversy," *Circ. Arrhythmia Electrophysiol.*, vol. 2, no. 1, pp. 80–88, 2010.

[21] E. Anyukhovsky, E. Sosunov, and M. Rosen, "Regional differences in electrophysiological properties of epicardium, midmyocardium, and endocardium. In vitro and in vivo correlations," *Circulation*, vol. 94, no. 8, pp. 1981–1988, 1996.

[22] G.-X. Yan and C. Antzelevitch, "Cellular Basis for the Normal T Wave and the the Long-QT Syndrome," *Circulation*, vol. 98, pp. 1928–1936,

1998.

[23] E. Anyukhovsky, E. Sosunov, R. Gainullin, and M. Rosen, "The controversial M cell," *J. Cardiovasc. Electrophysiol.*, vol. 10, no. 2, pp. 244–260, 1999.

[24] Y. Castro-Torres, "Ventricular repolarization markers for predicting malignant arrhythmias in clinical practice," *World J. Clin. Cases*, vol. 3, no. 8, p. 705, 2015.

[25] J. T. Tikkanen *et al.*, "Long-Term Outcome Associated with Early Repolarization on Electrocardiography," *N. Engl. J. Med.*, vol. 361, no. 26, pp. 2529–2537, 2009.

[26] M. Haïssaguerre *et al.*, "Sudden Cardiac Arrest Associated with Early Repolarization," *N. Engl. J. Med.*, vol. 358, no. 19, pp. 2016–2023, 2008.

[27] J. Siebermair *et al.*, "Early repolarization pattern is the strongest predictor of arrhythmia recurrence in patients with idiopathic ventricular fibrillation: results from a single centre long-term follow-up over 20 years," *Europace*, vol. 18, no. 5, pp. 718–725, 2016.

[28] Y. Cheng *et al.*, "Role of Early Repolarization Pattern in Increasing Risk of Death," *J. Am. Heart Assoc.*, vol. 5, no. 9, p. e003375, 2016.

[29] J. Zhang *et al.*, "The Electrophysiological Substrate of Early Repolarization Syndrome: Noninvasive Mapping in Patients," *JACC Clin. Electrophysiol.*, vol. 3, no. 8, pp. 894–904, 2017.

[30] J. Zhang *et al.*, "Cardiac electrophysiological substrate underlying the ECG phenotype and electrogram abnormalities in brugada syndrome patients," *Circulation*, vol. 131, no. 22, pp. 1950–1959, 2015.

[31] H. A. P. Peeters *et al.*, "Electrocardiographic identification of abnormal ventricular depolarization and repolarization in patients with idiopathic ventricular fibrillation," *J. Am. Coll. Cardiol.*, vol. 31, no. 6, pp. 1406–1413, 1998.

[32] A. Frustaci *et al.*, "Cardiac histological substrate in patients with clinical phenotype of Brugada syndrome," *Circulation*, vol. 112, no. 24, pp. 3680–3687, 2005.

[33] C. Pater, "Methodological considerations in the design of trials for safety assessment of new drugs and chemical entities," *Curr. Control. Trials Cardiovasc. Med.*, 2005.

[34] P. G. Postema *et al.*, "Founder mutations in the Netherlands: Familial idiopathic ventricular fibrillation and DPP6," *Netherlands Hear. J.*, vol.

19, pp. 290–296, 2011.

[35] A. R. M. Herman *et al.*, "Outcome of apparently unexplained cardiac arrest: Results from investigation and follow-up of the prospective cardiac arrest survivors with preserved ejection fraction registry," *Circ. Arrhythmia Electrophysiol.*, 2016.

[36] J. E. Burnes, B. Taccardi, R. S. MacLeod, and Y. Rudy, "Noninvasive ECG imaging of electrophysiologically abnormal substrates in infarcted hearts : A model study.," *Circulation*, vol. 101, no. 5, pp. 533–540, 2000.

[37] M. J. M. Cluitmans *et al.*, "In Vivo Validation of Electrocardiographic Imaging," *JACC Clin. Electrophysiol.*, vol. 3, no. 3, pp. 232–242, Mar. 2017.

[38] M. J. M. Cluitmans, R. L. M. Peeters, R. L. Westra, and P. G. A. Volders, "Noninvasive reconstruction of cardiac electrical activity: update on current methods, applications and challenges," *Netherlands Hear. J.*, vol. 23, no. 6, pp. 301–311, 2015.

[39] L. De Ambroggi and A. D. Corlan, "Clinical use of body surface potential mapping in cardiac arrhythmias," *Anadolu Kardiyol. Derg.*, vol. 7 Suppl 1, no. 1, pp. 8–10, 2007.

[40] C. Ramanathan, P. Jia, R. Ghanem, K. Ryu, and Y. Rudy, "Activation and repolarization of the normal human heart under complete physiological conditions.," *Proc. Natl. Acad. Sci. U. S. A.*, vol. 103, no. 16, pp. 6309–14, Apr. 2006.

[41] R. Vijayakumar *et al.*, "Electrophysiologic substrate in congenital long QT syndrome: Noninvasive mapping with electrocardiographic imaging (ECGI)," *Circulation*, 2014.

[42] S. Ghosh *et al.*, "Early repolarization associated with sudden death: Insights from noninvasive electrocardiographic imaging," *Hear. Rhythm*, 2010.

[43] M. J. M. Cluitmans, "Noninvasive reconstruction of cardiac electrical activity: Mathematical innovation, in vivo validation and human application (*Dissertation*)," University of Maastricht, 2016.

[44] C. Ramanathan, R. N. Ghanem, P. Jia, K. Ryu, and Rudy, "Noninvasive electrocardiographic imaging for cardiac electrophysiology and arrhythmia," *Nat. Med.*, vol. 10, no. 4, pp. 422–428, 2004.

[45] CIBC, "Seg3D: Volumetric Image Segmentation and Visualization. Scientific Computing and Imaging Institute (SCI), Download from:

http://www.seg3d.org".” 016.

[46] B. B. Punske *et al.*, “Mechanisms of the spatial distribution of QT intervals on the epicardial and body surfaces.,” *J. Cardiovasc. Electrophysiol.*, vol. 10, no. 12, pp. 1605–1618, 1999.

[47] M. J. M. Cluitmans, M. Clerx, N. Vandersickel, R. L. M. Peeters, P. G. A. Volders, and R. L. Westra, “Physiology-based regularization of the electrocardiographic inverse problem,” *Med. Biol. Eng. Comput.*, vol. 55, no. 8, pp. 1353–1365, 2017.

[48] SCI Institute, “SCIRun: A Scientific Computing Problem Solving Environment, Scientific Computing and Imaging Institute (SCI), Download from: http://www.scirun.org.” 2016.

[49] T. G. Neilan *et al.*, “Late gadolinium enhancement among survivors of sudden cardiac arrest,” *JACC Cardiovasc. Imaging*, 2015.

[50] P. Rodrigues *et al.*, “Diagnosis and Prognosis in Sudden Cardiac Arrest Survivors Without Coronary Artery Disease: Utility of a Clinical Approach Using Cardiac Magnetic Resonance Imaging,” *Circ. Cardiovasc. Imaging*, 2017.

[51] A. La Gerche *et al.*, “Cardiac imaging and stress testing asymptomatic athletes to identify those at risk of sudden cardiac death,” *JACC Cardiovasc. Imaging*, 2013.

[52] D. Corrado, C. Basso, and G. Thiene, “Sudden cardiac death in young people with apparently normal heart,” *Cardiovasc. Res.*, vol. 50, no. 2, pp. 399–408, 2001.

[53] M. Zhang *et al.*, “The role of focal myocardial inflammation in sudden unexpected cardiac and noncardiac deaths-A clinicopathological study,” *International Journal of Legal Medicine*. 2013.

[54] N. V. Arteyeva, S. L. Goshka, K. A. Sedova, O. G. Bernikova, and J. E. Azarov, “What does the Tpeak-Tendinterval reflect? An experimental and model study,” *J. Electrocardiol.*, vol. 46, no. 4, 2013.

[55] C. Antzelevitch and W. Shimizu, “Cellular mechanisms underlying the long QT syndrome,” *Curr.Opin.Cardiol.*, vol. 17, no. 0268–4705 SB–IM, pp. 43–51, 2002.

[56] J. M. Fish, J. M. Di Diego, V. Nesterenko, and C. Antzelevitch, “Epicardial Activation of Left Ventricular Wall Prolongs QT Interval and Transmural Dispersion of Repolarization: Implications for Biventricular Pacing,” *Circulation*, 2004.

[57] K. P. Letsas *et al.*, "Novel indexes of heterogeneity of ventricular repolarization in subjects with early repolarization pattern," *Europace*, 2012.

[58] A. Lubinski, E. Lewicka-Nowak, M. Kempa, A. M. Baczynska, I. Romanowska, and G. Swiatecka, "New Insight into Repolarization Abnormalities in Patients with Congenital Long QT Syndrome: the Increased Transmural Dispersion of Repoiarization," *Pacing Clin. Electrophysiol.*, vol. 21, no. 1, pp. 172–175, 1998.

[59] K. Takenaka *et al.*, "Exercise stress test amplifies genotype-phenotype correlation in the LQT1 and LQT2 forms of the long-QT syndrome," *Circulation*, vol. 107, no. 6, pp. 838–844, 2003.

[60] G. Tse *et al.*, "Meta-analysis of Tpeak-Tendand Tpeak-Tend/QT ratio for risk stratification in congenital long QT syndrome," *J. Electrocardiol.*, pp. 1–6, 2018.

[61] M. Yamaguchi *et al.*, "T wave peak-to-end interval and QT dispersion in acquired long QT syndrome: a new index for arrhythmogenicity," *Clin. Sci.*, vol. 105, no. 6, pp. 671–676, 2003.

[62] J. Castro Hevia *et al.*, "Tpeak-Tend and Tpeak-Tend Dispersion as Risk Factors for Ventricular Tachycardia/Ventricular Fibrillation in Patients With the Brugada Syndrome," *J. Am. Coll. Cardiol.*, vol. 47, no. 9, pp. 1828–1834, 2006.

[63] H. Morita, A. Watanabe, S. Kawada, and M. Miyamoto, "Identification of electrocardiographic risk markers for the initial and recurrent episodes of ventricular fibrillation in patients with Brugada syndrome," *J. Cardiovasc. Electrophysiol.*, vol. 29, pp. 107–114, 2018.

[64] G. Mugnai *et al.*, "Role of Electrocardiographic Tpeak-Tend for the Prediction of Ventricular Arrhythmic Events in the Brugada Syndrome," *Am. J. Cardiol.*, vol. 120, no. 8, pp. 1332–1337, 2017.

[65] B. D. Nearing, G. A. Wellenius, M. A. Mittleman, M. E. Josephson, A. J. Burger, and R. L. Verrier, "Crescendo in Depolarization and Repolarization Heterogeneity Heralds Development of Ventricular Tachycardia in Hospitalized Patients with Decompensated Heart Failure," *Circ. Arrhythmia Electrophysiol.*, vol. 5, no. 1, pp. 84–90, 2013.

[66] T. V. Kenttä *et al.*, "Prediction of sudden cardiac death with automated high-throughput analysis of heterogeneity in standard resting 12-lead electrocardiograms," *Hear. Rhythm*, vol. 13, no. 3, pp. 713–720, 2016.

[67] M. Zabel, S. Portnoy, and M. R. Franz, "Electrocardiographic indexes of dispersion of ventricular repolarization: An isolated heart validation study," *J. Am. Coll. Cardiol.*, vol. 25, no. 3, pp. 746–752, 1995.

[68] N. V. Arteyeva and J. E. Azarov, "Effect of action potential duration on Tpeak-Tendinterval, T-wave area and T-wave amplitude as indices of dispersion of repolarization: Theoretical and simulation study in the rabbit heart," *J. Electrocardiol.*, vol. 50, no. 6, pp. 919–924, 2017.

[69] T. V. Kenttä *et al.*, "Repolarization Heterogeneity Measured With T-Wave Area Dispersion in Standard 12-Lead ECG Predicts Sudden Cardiac Death in General Population," *Circ. Arrhythmia Electrophysiol.*, vol. 11, no. 2, p. e005762, 2018.

[70] R. L. Verrier *et al.*, "Microvolt T-wave alternans physiological basis, methods of measurement, and clinical utility -- consensus guideline by International Society for Holter and Noninvasive Electrocardiology," *J. Am. Coll. Cardiol.*, vol. 58, no. 13, pp. 1309–1324, 2011.

[71] G. Tse and B. P. Yan, "Traditional and novel electrocardiographic conduction and repolarization markers of sudden cardiac death," *EP Eur.*, vol. 19, no. 5, pp. 712–721, 2017.

[72] D. M. Bloomfield *et al.*, "Microvolt T-wave alternans and the risk of death or sustained ventricular arrhythmias in patients with left ventricular dysfunction," *J. Am. Coll. Cardiol.*, vol. 47, no. 2, pp. 456–463, 2006.

[73] F. M. Merchant, O. Sayadi, K. Moazzami, D. Puppala, and A. Amoundas, "T-wave alternans as an arrhythmic risk stratifier: state of the art," *Current Cardiology Reports,* 2013.

[74] L. G. Tereshchenko and M. E. Josephson, "Frequency content and characteristics of ventricular conduction," *J. Electrocardiol.*, vol. 48, no. 6, pp. 933–937, 2015.

[75] K. L. Park, K. J. Lee, and H. R. Yoon, "Application of a wavelet adaptive filter to minimise distortion of the ST-segment," *Med. Biol. Eng. Comput.*, vol. 36, no. 5, pp. 581–586, 1998.

[76] A. A. Suraj, M. Francis, T. S. Kavya, and T. M. Nirmal, "Discrete wavelet transform based image fusion and de-noising in FPGA," *J. Electr. Syst. Inf. Technol.*, vol. 1, no. 1, pp. 72–81, 2014.

[77] G. F. Salles, C. R. L. Cardoso, S. M. Leocadio, and E. S. Muxfeldt, "Recent ventricular repolarization markers in resistant hypertension: Are they different from the traditional QT interval?," *Am. J. Hypertens.*, vol.

21, no. 1, pp. 47–53, 2008.

[78] K. S. Kumar, B. Yazdanpanah, and P. R. Kumar, "Removal of noise from electrocardiogram using digital FIR and IIR filters with various methods," in *2015 International Conference on Communication and Signal Processing, ICCSP 2015*, 2015.

[79] D. Panigrahy and P. K. Sahu, "P and T wave detection and delineation of ECG signal using differential evolution (DE) optimization strategy," *Australas. Phys. Eng. Sci. Med.*, vol. 41, no. 1, pp. 225–241, 2018.

[80] P. De Chazal, C. Heneghan, E. Sheridan, R. Reilly, P. Nolan, and M. O'Malley, "Automated processing of the single-lead electrocardiogram for the detection of obstructive sleep apnoea," *IEEE Trans. Biomed. Eng.*, vol. 50, no. 6, pp. 686–696, 2003.

[81] Z. Liu, J. Wang, and B. Liu, "ECG signal denoising based on morphological filtering," *5th Int. Conf. Bioinforma. Biomed. Eng. iCBBE 2011*, pp. 2–5, 2011.

[82] L. S. Correa, E. Laciar, A. Torres, and R. Jane, "Performance evaluation of three methods for respiratory signal estimation from the electrocardiogram," in *2008 30th Annual International Conference of the IEEE Engineering in Medicine and Biology Society*, 2008, pp. 4760–4763.

[83] L. Suyi and L. Jun, "The optimal de-noising algorithm for ECG using stationary wavelet transform," *2009 WRI World Congr. Comput. Sci. Inf. Eng. CSIE 2009*, vol. 6, no. 2007, pp. 469–473, 2009.

[84] G. Lenis, N. Pilia, A. Loewe, W. H. W. Schulze, and O. Dössel, "Comparison of Baseline Wander Removal Techniques considering the Preservation of ST Changes in the Ischemic ECG: A Simulation Study," *Comput. Math. Methods Med.*, vol. 2017, 2017.

[85] W. Dai, I. Selesnick, J.-R. Rizzo, J. Rucker, and T. Hudson, "A nonlinear generalization of the Savitzky-Golay filter and the quantitative analysis of saccades," *J. Vis.*, vol. 17, no. 9, p. 10, 2017.

[86] G. Vivó-Truyols and P. J. Schoenmakers, "Automatic selection of optimal Savitzky-Golay smoothing," *Anal. Chem.*, vol. 78, no. 13, pp. 4598–4608, 2006.

[87] P. M. Rautaharju, B. Surawicz, and L. S. Gettes, "AHA/ACCF/HRS Recommendations for the Standardization and Interpretation of the Electrocardiogram. Part IV: The ST Segment, T and U Waves, and the QT Interval A Scientific Statement From the American Heart Association

Electrocardiography and Arrhythmias Committee, Council on Clinical Cardiology; the American College of Cardiology Foundation; and the Heart Rhythm Society," *Journal of the American College of Cardiology*. 2009.

[88] M. Cesari, J. Mehlsen, A. B. Mehlsen, and H. B. D. Sorensen, "A New Wavelet-Based ECG Delineator for the Evaluation of the Ventricular Innervation," *IEEE J. Transl. Eng. Heal. Med.*, vol. 5, no. June, 2017.

[89] K. Sembulingam and P. Sembulingam, *Essentials of Medical Physiology*, 6th ed. London, U.K.: J.P. Medical, 2012.

[90] V. M. F. Meijborg, C. E. Conrath, T. Opthof, C. N. W. Belterman, J. M. T. De Bakker, and R. Coronel, "Electrocardiographic T wave and its relation with ventricular repolarization along major anatomical axes," *Circ. Arrhythmia Electrophysiol.*, vol. 7, no. 3, pp. 524–531, 2014.

[91] B. Charbit, E. Samain, P. Merckx, and C. Funck-Brentano, "QT Interval Measurement," *Anesthesiology*, vol. 104, no. 2, pp. 255–260, 2006.

[92] P. G. Postema, J. S. S. G. De Jong, I. A. C. Van der Bilt, and A. A. M. Wilde, "Accurate electrocardiographic assessment of the QT interval: Teach the tangent," *Hear. Rhythm*, vol. 5, no. 7, pp. 1015–1018, 2008.

[93] E. Lepeschkin and B. Surawicz, "The measurement of the QT interval of the electrocardiogram," *Circulation*, vol. 6, no. 3, pp. 378–388, 1952.

[94] G. Erikssen, K. Liestøl, L. Gullestad, K. H. Haugaa, B. Bendz, and J. P. Amlie, "The terminal part of the QT interval (T peak to T end): A predictor of mortality after acute myocardial infarction," *Ann. Noninvasive Electrocardiol.*, vol. 17, no. 2, pp. 85–94, 2012.

[95] E. J. da S. Luz, W. R. Schwartz, G. Cámara-Chávez, and D. Menotti, "ECG-based heartbeat classification for arrhythmia detection: A survey," *Comput. Methods Programs Biomed.*, vol. 127, pp. 144–164, 2016.

[96] J. P. Martínez, R. Almeida, S. Olmos, A. P. Rocha, and P. Laguna, "A wavelet-based ECG delineator: evaluation on standard databases.," *IEEE Trans. Biomed. Eng.*, vol. 51, no. 4, pp. 570–581, 2004.

[97] CSE Working Party, "Recommendations for measurement standards in quantitative electrocardiography," *Eur. Heart J.*, vol. 6, no. 10, pp. 815–825, 1985.

[98] S. M. Kim *et al.*, "The pattern of tpeak-tend and QT interval, and J wave during therapeutic hypothermia," *J. Electrocardiol.*, vol. 47, no. 1, pp. 84–92, 2014.

[99] CART-Tech Utrecht, "CARTBox." 2017.

[100] Y. Sun, K. L. Chan, and S. M. Krishnan, "ECG signal conditioning by morphological filtering," *Comput. Biol. Med.*, vol. 32, no. 6, pp. 465–479, 2002.

[101] J. M. Bote, J. Recas, F. Rincon, D. Atienza, and R. Hermida, "A Modular Low-Complexity ECG Delineation Algorithm for Real-Time Embedded Systems," *IEEE J. Biomed. Heal. Informatics*, vol. 22, no. 2, pp. 429–441, 2018.